Journal of Earth Science, *Vol. 32*, *No. 6*, *p. 1300–1331*, *December 2021* *ISSN 1674-487X*
Printed in China
https://doi.org/10.1007/s12583-021-1462-7

A Comparison between the ~1.08–1.13 Ga Volcano-Sedimentary Koras Group and Plutonic Keimoes Suite: Insights into the Post-Collisional Tectono-Magmatic Evolution of the Eastern Namaqua Metamorphic Province, South Africa

Russell Bailie*, Aidan Leetz
Department of Earth Sciences, *University of the Western Cape*, *Bellville*, *Cape Town*, *South Africa*
Russell Bailie: https://orcid.org/0000-0002-6119-1563; Aidan Leetz: https://orcid.org/0000-0001-8983-8552

ABSTRACT: Along the eastern margin of the Mesoproterozoic Namaqua metamorphic province (NMP) of southern Africa are a bimodal volcano-sedimentary succession, the ~1.13–1.10 Ga Koras Group, composed of rhyolitic porphyries and basaltic andesites, and the ~1.11–1.07 Ga late- to post-tectonic granitoids of the Keimoes Suite. This review examines existing whole-rock major- and trace-element data, along with isotope chemistry (with some new isotopic data), to investigate the role these two magmatic successions played in terms of post-collisional magmatism of the eastern NMP near the boundary with the Archean Kaapvaal Craton. The Keimoes Suite comprises variably porphyritic biotite monzogranites and granodiorites, with a charnockitic member. They are metaluminous to weakly peraluminous, ferroan, and calc-alkalic. They exhibit large ion lithophile (LIL) element enrichment relative to the high field strength elements (HFSE) with depletions in Ba, Sr, Nb, P, Eu and Ti, and enrichments in Th, U and Pb. Isotopic values ($\varepsilon_{Nd}(t)$: 2.78 to -2.95, but down to -8.58 for one granite, depleted mantle Nd model ages (T_{DM}): 1.62–1.99 Ga, but up to 2.55 Ga; initial $^{87}Sr/^{86}Sr$: 0.652 82–0.771 30) suggest derivation from weakly to mildly enriched (and radiogenic) sources of Meso- to Paleoproterozoic age, the former of more juvenile character. The Koras Group is characterized by a bimodal succession of calcic to calc-alkalic, magnesian and tholeiitic basaltic andesites and mostly metaluminous to peralkaline rhyolitic porphyries. Two successions are recognised, an older, lower succession that extruded at ~1.13 Ga, and a younger, upper succession at ~1.10 Ga. The rhyolitic porphyries of both successions show similar LILE/HFSE enrichment and the same element enrichments and depletions as the Keimoes Suite granitoids. The upper succession is consistently more fractionated in terms of both whole-rock major and trace element chemistry, and, isotopically, has a greater enriched source component ($\varepsilon_{Nd}(t)$: -0.69 to -4.26; T_{DM}: 1.64–2.44 Ga), relative to the lower succession ($\varepsilon_{Nd}(t)$: 0.74–5.62; T_{DM}: 1.28–2.12 Ga). Crystal fractionation of plagioclase and K-feldspar appears to have played a role in bringing about compositional variation in many of the granites. These were derived from partial melting of mainly igneous with subordinate sedimentary sources from mostly lower crustal depths, although some granitoids have indications of a possible mantle source component. The lower succession of the Koras Group was derived by partial melting of subduction-influenced enriched mantle giving rise to mafic magmas that fractionated to give rise to the rhyolitic porphyries. The upper succession rhyolites were derived by crustal melting due to the input of mafic magmatism. Crystal fractionation was the main compositional driver for both successions. The Keimoes Suite granitoids and the Koras Group are associated with extensional regimes subsequent to the main deformational episode in the eastern NMP.

KEY WORDS: rhyolitic porphyries and basaltic andesites, megacrystic late- to post-tectonic granitoids, whole-rock chemistry, isotopes, crystal fractionation.

0 INTRODUCTION

Volcanic and plutonic rocks are important in understanding the processes that give rise to a substantial amount of the continental crust (e.g., Yan et al., 2018a, b; Barth et al., 2012; Gagnevin et al., 2010; Bachmann et al., 2007). Post-collisional magmatism forms an important component of magmatism associated with continental collisional and accretionary events. The role of structures and deformation in generating post-collisional magma-

*Corresponding author: rbailie@uwc.ac.za

Manuscript received September 25, 2020.
Manuscript accepted March 25, 2021.

Bailie, R., Leetz, A., 2021. A Comparison between the ~1.08–1.13 Ga Volcano-Sedimentary Koras Group and Plutonic Keimoes Suite: Insights into the Post-Collisional Tectono-Magmatic Evolution of the Eastern Namaqua Metamorphic Province, South Africa. *Journal of Earth Science*, 32(6): 1300–1331. https://doi.org/10.1007/s12583-021-1462-7. http://en.earth-science.net

tism is also of significance in understanding the sources and plumbing system for the magmatism (e.g., Seghedi et al., 2019). The ~1.13–1.10 Ga bimodal volcano-sedimentary Koras Group, and the ~1.11–1.08 Ga plutonic Keimoes Suite granitoids represent voluminous post-collisional magmatism in the eastern Namaqua metamorphic province (NMP) of southern Africa subsequent to the major collisional, accretionary and deformational events associated with the 1.2–1.0 Ga Namaquan Orogeny. The Keimoes Suite constitutes weakly foliated to unfoliated, medium- to coarse-grained late- to post-tectonic I-type megacrystic granites and charnockites. These biotite-bearing, ferroan, alkali-calcic granitoids intruded within a collisional within-plate tectonic setting (Bailie et al., 2017, 2011a). The Koras Group was extruded in two stages, initially at ~1.13 Ga (Mothibi, 2016), and later at ~1.10 Ga (Bailie et al., 2012; Pettersson et al., 2007). The Koras Group lithologies originate from A-type parental magmas (Bailie et al., 2012), whilst the Keimoes Suite has essentially I-type characteristics, but the high Fe/Mg ratios, as well as high large ion lithophile element (LILE), rare earth elements (REE), and high field strength element (HFSE) contents are suggestive of A-type granites.

A number of workers in the region (Bailie et al., 2012; Pettersson et al., 2007; Moen, 1987) have suggested that the two are potentially related, with one being the extrusive equivalent of the other, based on their similar ages and whole-rock chemistry. Their temporal and spatial separation, however, tends to preclude such an association. Together, however, they represent an extensive late- to post-tectonic magmatic event within the eastern NMP at ~1.13–1.08 Ga. This review re-examines the textural, whole-rock chemistry and isotopic characteristics of these rocks in order to provide further constraints on their sources, petrogenesis and causes of this extensive post-collisional magmatism. It also seeks to provide further constraints on the tectonomagmatic evolution of the eastern NMP at this time during the 1.2–1.0 Ga Namaquan Orogeny.

1 GEOLOGICAL SETTING

The Namaqua-Natal metamorphic province (NNMP) is a medium to high-grade metamorphic belt which borders the Archean Kaapvaal Craton of southern Africa to its southeast, south and west (Cornell et al., 2006). The NNMP is composed of para- and ortho-gneisses formed, deformed and metamorphosed during the 1.2–1.0 Ga Namaquan Orogeny, and is potentially associated with the assembly of the supercontinent Rodinia (Jacobs et al., 2008; Li et al., 2008). The Namaqua metamorphic province (NMP) forms the western portion of the greater NNMP to the west of the Kaapvaal Craton (Fig. 1).

The NMP can be divided into five distinct domains, each characterized by its own distinctive lithostratigraphy and structural fabric. The term domain is used in preference to terrane, because the latter has tectonic implications, whereas the former is more generic and non-tectonic or origin-based. These domains are, from west to east (Fig. 1): the Bushmanland Subprovince (BSP), itself composed of a number of smaller domains, the Richtersveld magmatic arc (RMA), the Kakamas Domain (KD), the Areachap Domain (AD), and the Kheis terrane on the western margin of the Kaapvaal Craton (Van Niekerk and Beukes, 2019).

The Kakamas Domain is dominated by poly-deformed ortho- and para-gneisses and is bound between the Boven Rugzeer shear zone (BoSZ) to the east and the Hartbees River thrust to the west (Fig. 1; Cornell et al., 2006). It comprises ~1.2–1.15 Ga granulite facies supracrustal rocks (Pettersson et al., 2007) and ~1.21–1.15 Ga pre- to syn-tectonic granitic gneisses intruded by the later ~1.11–1.07 Ga late- to post-tectonic Keimoes Suite (Bailie et al., 2017). The domain is considered to be a low-angle imbricate mega-nappe stack bounded by major thrust structures, e.g., Macey et al. (2017).

The Areachap Domain comprises poly-deformed mafic to intermediate volcano-sedimentary gneisses with a calc-alkaline arc-like affinity termed the Areachap Group of ~1.24–1.29 Ga age (Bailie et al., 2010; Cornell and Pettersson, 2007; Pettersson et al., 2007; Cornell et al., 1990). The Areachap Group was subjected to upper amphibolite facies metamorphism to the north, and lower granulite facies metamorphism to the south. The northern part, in particular, is characterized by a greater dominance of Paleoproterozoic model ages (Cornell and Pettersson, 2007; Pettersson et al., 2007) suggesting an older crustal component was present toward the northern end of the magmatic arc(s) that gave rise to the Areachap Group (Pettersson et al., 2009). This succession separates the western, granitoid-dominated NMP from the arenitic meta-sedimentary and volcanic rocks of the ~1.92–1.3 Ga Kheis terrane (Van Niekerk, 2006). The granitoids of the Keimoes Suite extensively intruded the Areachap Group. The BoSZ represents the western boundary with the Kakamas Domain, with the eastern boundary being the Trooilapspan shear zone (TLSZ) and Brakbosch fault (Cornell et al., 2006; Fig. 1). The exposures of the Areachap Group north of Upington are unconformably overlain by rocks belonging to the Koras Group (Fig. 2; Bailie et al., 2012). The Koras Group is, however, far more widespread in the adjacent Kheis terrane. The western NMP is characterised, in general, by a greater Paleoproterozoic signature in Nd model ages (Eglington, 2006) compared to the more juvenile eastern NMP (Pettersson et al., 2009). Both the Areachap and Kakamas domains were intruded by both ~1.19–1.15 Ga pre- to syn-tectonic granitic gneisses, and later ~1.11–1.08 Ga late- to post-tectonic granites, the latter comprising the Keimoes Suite (Bailie et al., 2017, 2011a), during the Namaquan Orogeny.

Van Niekerk and Beukes (2019) argued that the former Kaaien terrane and Kheis Subprovince (e.g., Cornell et al., 2006) be combined into the Kheis terrane, and all the rocks therein be grouped into the proposed ~1.92–1.35 Ga Keis Supergroup (Fig. 2). The eastern boundary of the Kheis terrane is defined by the ~1.20 Ga Blackridge thrust (Evans et al., 2001). The Brakbosch-Trooilapspan shear zone acts as the western boundary of the Kheis terrane (Figs. 1, 2), becoming the north-south oriented aeromagnetic signature termed the Kalahari line further north. All the successions east of the Trooilapspan-Brakbosch fault/shear zone form the western margin of the Kaapvaal Craton. The Keis Supergroup represents passive margin sediments and comprises meta-arenaceous, shale and schistose units (Van Niekerk and Beukes, 2019), capped by a bimodal volcanic unit (the Leerkrans Formation of the Wilgenhoutsdrif Group; Fig. 2). All these are in sedimentary contact with each rather than in tectonic contact, as

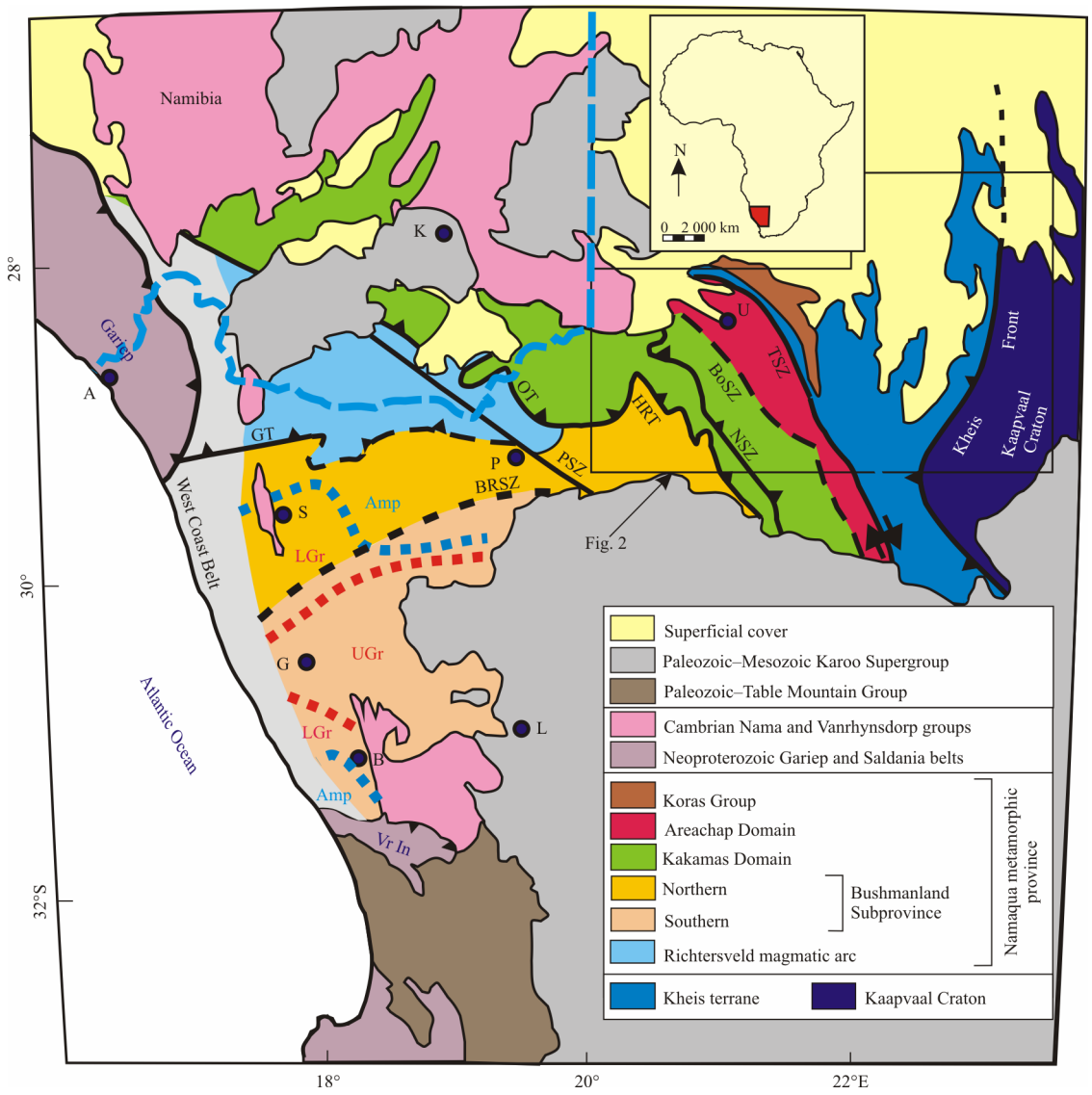

Figure 1. Simplified geological map of the Namaqua metamorphic province (NMP) of the Namaqua-Natal metamorphic province (taken from Macey et al., 2011; modified after Thomas et al., 1994; Moen and Toogood, 2007). The inset shows the position of the larger map in Africa. Towns: A. Alexander Bay; B. Bitterfontein; G. Garies; K. Karasburg; L. Loeriesfontein; P. Pofadder; S. Springbok; U. Upington; metamorphic facies indicators: Amp. amphibolite; LGr. lower granulite; UGr. upper granulite; structural features: BoSZ. Boven Rugzeer shear zone; BRSZ. Buffels River shear zone; GT. Groothoek thrust; HRT. Hartbees River thrust; NSZ. Neusspruit shear zone; OT. Onseepkans thrust; PSZ. Pofadder shear zone; TSZ. Trooilapspan shear zone; Vr In. Vanrhynsdorp Inlier.

previously advocated (e.g., Moen, 1999). These units are unconformably overlain by the Koras Group. The uppermost Wilgenhoutsdrif Group marked a transition to an active continental plate margin and development of an intra-continental back-arc setting behind the Areachap volcanic arc along the western margin of the Kaapvaal Craton (Bailie et al., 2011b; Pettersson et al., 2007), with easterly-directed subduction (Van Niekerk, 2006).

The Kheis terrane was subjected to east-west-directed shortening, resulting in alternating NW-SE-oriented anticlines and synclines; shortening is bracketed between 1 200 and 1 150 Ma (Van Niekerk and Beukes, 2019). The Kakamas and Areachap domains were thrust eastwards over the Kheis terrane at ~1.24–1.20 Ga (Eglington, 2006) at the onset of the 1.2–1.0 Ga Namaquan Orogeny with the closure of the Areachap Sea/Ocean and the accretion of the Areachap arc onto the western margin of the Kaapvaal Craton (e.g., Pettersson et al., 2007).

In the Kakamas and Areachap domains four major deformational events are recognised. The first deformation event, D_1, is subdivided into two sub-events, D_{1a} that occurred at ~1 200 Ma, and D_{1b}, at ~1 170–1150 Ma (Mathee, 2017). The main D_2 event gave rise to large-scale tight to isoclinal, non-cylindrical sub-vertical F_2 folds with NW-trending fold axes, as well as thrusts. This deformation event is constrained to have occurred at ~1 120–1 100 Ma (Bailie et al., 2017; Mathee, 2017). The F_1 and F_2 folding events were the main regional penetrative fabric-forming events. The third event (D_3) occurred at ~1 075–1 080 Ma, and gave rise to open east-west-trending upright F_3 folds. Subsequent D_4 deformation, constrained to have occurred between 1 024 and 1 018 Ma (Mathee, 2017), is characterized by reactivation and steepening of intra-terrane thrusts by transpression as sub-vertical dextral shear zones with both a lateral and vertical displacement (Pettersson et al., 2007). These in-

clude the BoSZ, TLSZ and Brakbosch shear zone, which, while likely formed during D_2 fold and thrust tectonics, show evidence for extensive reactivation, as well as vertical and lateral movement (e.g., van Bever Donker, 1991, 1980).

The peak metamorphic event (M_2) occurred at ~1 170–1 150 Ma, with upper amphibolite to granulite facies conditions in the Kakamas Domain (800–850 °C at 4–4.5 kbar) but varying to lower amphibolite facies conditions (550 °C, 1.5–2.5 kbar)

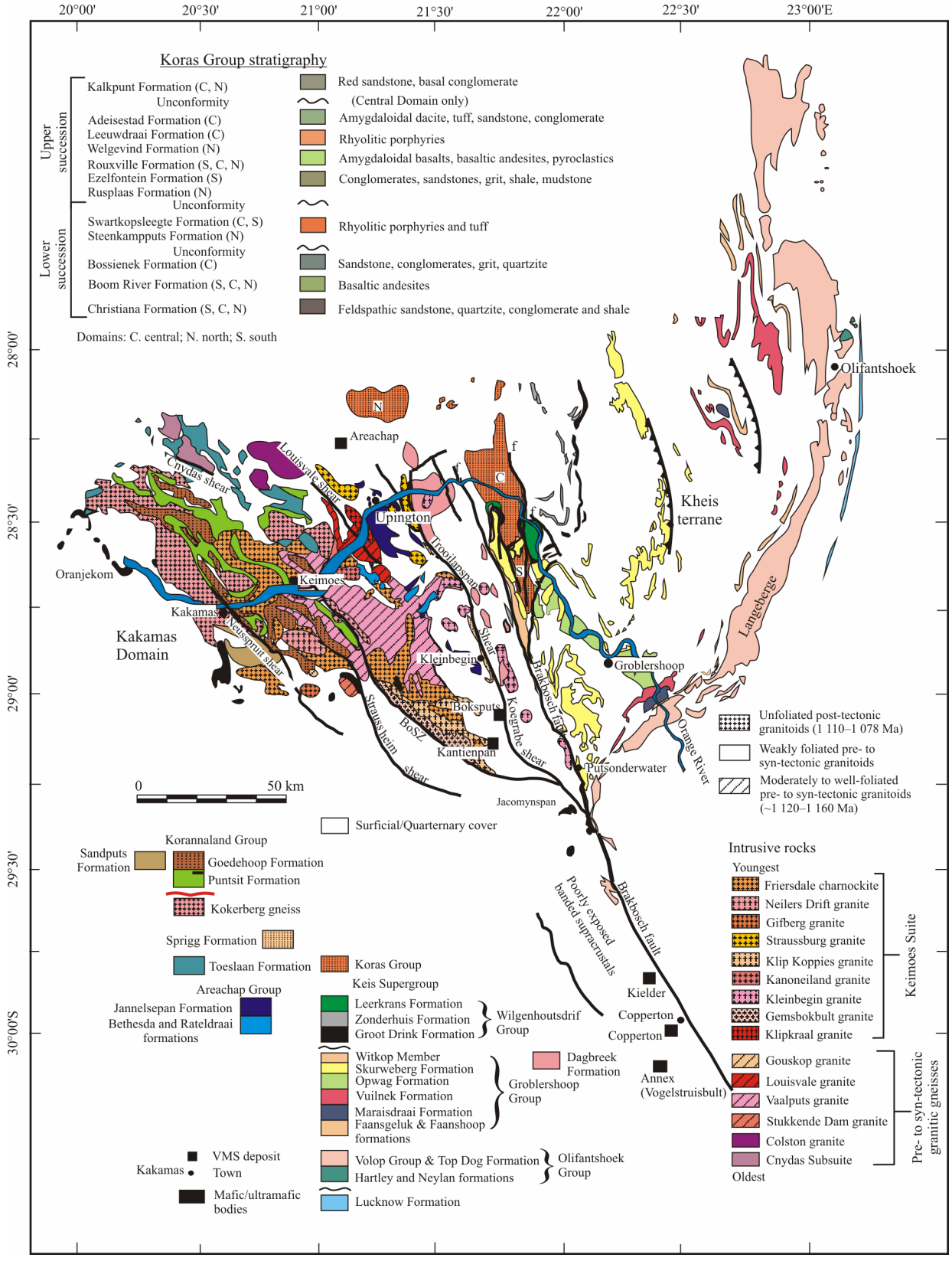

Figure 2. Geological map of the eastern NMP adjacent to the western margin of the Archean Kaapvaal Craton. The Koras Group and its stratigraphy are indicated along with the various granitoids comprising the loosely defined Keimoes Suite.

along regions adjacent to the BoSZ in the Areachap Domain (Cornell et al., 2006; Humphreys and van Bever Donker, 1990; Stowe, 1983). This was mostly due to the intrusion of the pre- to syn-tectonic granitic gneisses. M_3 metamorphism occurred at amphibolite facies conditions (~650 °C and 6.5 kbar; Bachmann et al., 2015) and accompanied D_3 deformation. It was a retrograde to isothermal regional contact metamorphic event associated with intrusion of the Keimoes Suite at ~1.11–1.08 Ga. D_4 deformation was associated with M_4 retrograde metamorphism, concentrated especially along dextral shear zones (Pettersson et al., 2007; Cornell et al., 2006; Geringer et al., 1994; van Bever Donker, 1980).

The lithologies of the Kheis terrane, apart from the Koras Group, experienced three episodes of deformation. The first phase of deformation (D_1) resulted in isoclinal folding, with the second event (D_2) producing folds that refolded the F_1 folds. The third event, D_3, is associated with large scale dextral shear movement. The Keis Supergroup experienced low-grade metamorphism (400–480 °C, 1 kbar), except along the Brakbosch shear zone where higher pressures up to 4 kbar were experienced. Prograde metamorphism was associated with D_1 and D_2 deformation. The Koras Group is essentially mildly deformed and has been metamorphosed to greenschist facies (Moen, 1987).

The 1.11–1.08 Ga Keimoes Suite is a group of mostly medium-grained porphyritic or megacrystic intrusions that have compositions ranging from granodioritic to potassic granite (Bailie et al., 2017; Cornell et al., 2012). The suite is dominantly composed of metaluminous, ferroan, calcic to calc-alkalic biotite monzogranites with generally high K_2O contents (Bailie et al., 2017, 2011a). They are locally hornblende- and orthopyroxene-bearing with moderate SiO_2 contents and arc-like affinities (LILE-enrichment relative to the HFSE, negative Ta-Nb, Ti and P anomalies). All these suggest an I-type nature. They, however, also have high Fe/Mg ratios, along with high HFSE, LILE and REE contents more indicative of A-type granites. The general trend of the suite is in a NW-SE orientation sub-parallel to the major F_2 fabric in the Kakamas and Areachap domains, and is confined to the area between the Neusspruit shear zone in the Kakamas Domain, and the Brakbosch fault (Fig. 2; Bailie et al., 2017). The Keimoes Suite straddles the boundary between the Areachap and Kakamas domains, being mostly restricted to in and around the BoSZ, which may have played a role in its emplacement (Bailie et al., 2017). It is more voluminous and widespread in the Areachap Domain. The granitoids intrude the Keis Supergroup and Areachap Group of the Areachap Domain, and the Korannaland Group of the Kakamas Domain, as well as older gneisses on a regional scale (Moen, 2007; Geringer et al., 1988).

The Koras Group is an ~7 000 m thick subalkaline bimodal volcanic succession characterised by calcic to calc-alkalic, magnesian and tholeiitic basaltic andesites along with mostly metaluminous rhyolitic porphyries, both of which are sandwiched between siliciclastic sediments (mostly sandstones, conglomerates, mudstones and feldspathic sandstones). It outcrops to the east of the Brakbosch fault in the Kheis terrane and is exposed in three domains with the domains comprising certain formations which are correlatives of each other (Figs. 1, 2). The stratigraphy of the succession is given in Fig. 2. The Koras Group comprises two successions (Fig. 2), with the lower succession extruded at ~1.13 Ga (Mothibi, 2016), and the upper succession occurring later at ~1.10 Ga (Bailie et al., 2012; Pettersson et al., 2007). Previous age determinations of the lower succession (Pettersson et al., 2007; Gutzmer et al., 2000) gave an ~1 170 Ma age. Recent age determinations (Mothibi, 2016), however, give a younger age of ~1 130 Ma, more in keeping with the largely undeformed nature of the group. Meter-scale folds, deformation fabrics, and slicken-sided striations, along with lower greenschist facies mineral assemblages, indicate that the Koras Group is not totally undeformed or unmetamorphosed (Moen, 1987; Sanderson-Damstra, 1982).

Temporal regional correlatives of the Koras Group and Keimoes Suite include the anorthositic gabbroic Oranjekom Complex intruded at ~1 100 Ma toward the western boundary of the Kakamas Domain (Kruger et al., 2000; Fig. 2). Isotopic data suggests a depleted mantle source for this complex.

2 METHODOLOGY

This review mostly uses previously published data to assess the origins, sources and petrogenesis of the Koras Group and Keimoes Suite. These include the whole-rock data published by Bailie et al. (2017, 2011a) for the Keimoes Suite, and that of Bailie et al. (2012) for the Koras Group. Analytical techniques for the Keimoes Suite are those of Bailie et al. (2017, 2011a), and for the Koras Group that of Bailie et al. (2012). The methods used to determine the isotopic ratios of the Keimoes Suite samples are from Bailie et al. (2017). Six new additional samples of the Koras Group were analysed for Sr-Nd isotopes due to lacking Rb-Sr isotopes (Bailie et al., 2012). All analytical techniques are given in ESM1.

3 LITHOLOGICAL DESCRIPTION

The lithologies of both successions are briefly described here, with more details given in Table S1 (ESM3).

3.1 Koras Group

The volcanic portion of the Koras Group is composed of basaltic andesites, rhyolitic porphyries and dacites. The dacites contain quartz and plagioclase phenocrysts with epidote- and quartz-filled amygdales (0.6–6 mm in size) within a fine-grained groundmass, whilst the basaltic andesites comprise skeletal plagioclase, ophitic augite, quartz, and epidotised and chloritised pyroxene phenocrysts in a fine-grained groundmass of plagioclase and augite (Fig. 3a). The metabasalts of the Rouxville Formation are amygdaloidal and contain quartz- and epidote-filled amygdales (1.4–16 mm) in a microcrystalline groundmass (65%) containing augite and lath-shaped plagioclase. The rhyolitic porphyries are composed of quartz, sanidine, plagioclase and chlorite phenocrysts and microphenocrysts within a fine-grained devitrified groundmass with microcrystalline quartz and plagioclase (45%–65%) (Figs. 3b–3d).

3.2 Keimoes Suite

The Keimoes Suite comprises the Gemsbokbult, Kanoneiland, Keboes, Klipkraal, Kleinbegin, Klip Koppies and Straussburg granites, along with the Friersdale charnockite. These megacrystic biotite granites are dominated by quartz

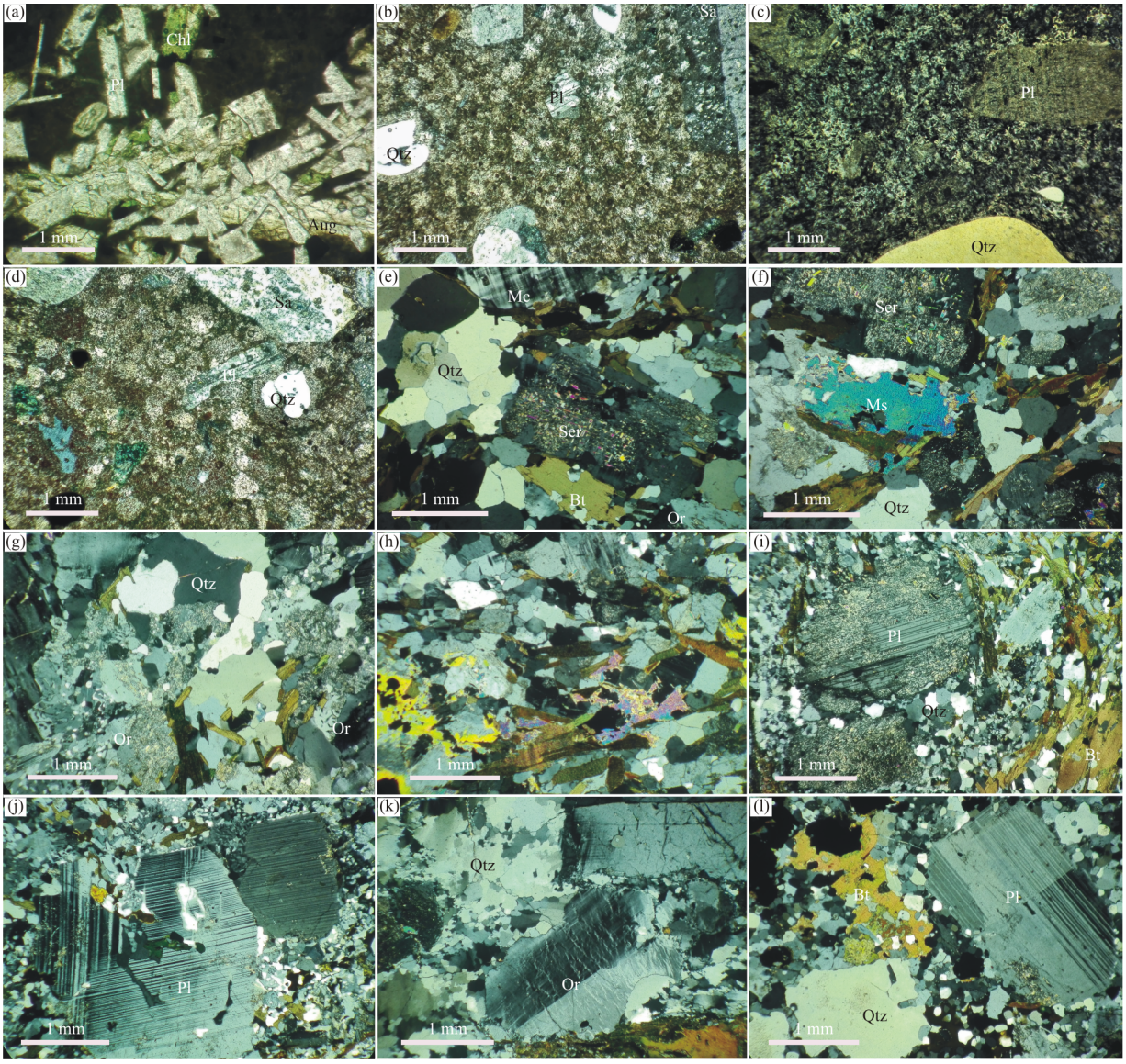

Figure 3. Petrographic photomicrographs of some of the bimodal volcanic rocks from the two successions of the Koras Group (a)–(d). (a) Basaltic andesite from the Boom River Formation, lower succession (sample K11); (b) rhyolitic porphyry from the Swartkopsleegte Formation, lower succession (sample K9); (c) rhyolitic porphyry from the Leeuwdraai Formation, upper succession (sample K13); (d) rhyolitic porphyry from the Welgevind Formation, upper succession (sample K36). Petrographic photomicrographs of the various granites of the Keimoes Suite (e)–(l). (e) Keboes granite (sample Mkb3); (f) Keboes granite (sample Mkb3); (g) Kanoneiland granite (sample Mka7); (h) Gemsbokbult granite (sample Mge4); (i) Klip Koppies granite (sample Mks1); (j) Klipkraal granite (sample Mkl5); (k) Straussburg granite (sample Ms2); (l) Friersdale charnockite (sample Mf7). Mineral abbreviations: Aug. augite; Bt. biotite; Chl. chlorite; Mcl. microcline; Ms. muscovite; Or. orthoclase; Pl. plagioclase; Qtz. quartz; Sa. sanidine; Ser. sericite.

(25%–40%), K-feldspars: orthoclase (12%–30%), and microcline (5%–10%), and plagioclase (5%–35%), with the dominant mafic mineral being biotite (5%–20%), with minor hornblende (2%–5%) present in some granites. The granites vary from unfoliated to poorly foliated. In some of the granites, namely the Gemsbokbult, Kanoneiland, Keboes and Kleinbegin granites, muscovite (1%–15%) is present, but is more prevalent in areas where shear zones crosscut the granites. Clinopyroxene, ranging in size from 0.2–2.4 mm, occurs in the Friersdale charnockite in limited amounts (1%–5%).

The Gemsbokbult granite is unfoliated to weakly foliated and mostly non-porphyritic with scattered phenocrysts, and has a medium-grained equigranular texture (Fig. 3h). Minor subhedral staurolite is associated with biotite. The Kanoneiland granite is medium- to coarse-grained, non-porphyritic and weakly foliated, varying in texture from inequigranular to equigranular (Fig. 3g). The Keboes granite is porphyritic and fine- to medium-grained (Fig. 3f). The Klipkraal granite is a porphyritic medium- to coarse-grained biotite granite with large orthoclase and plagioclase phenocrysts (Fig. 3j). The Kleinbegin granite, the dominant granite of the Kleinbegin Subsuite (Bailie et al., 2017, 2011a), has two main varieties, being either porphyritic or non-porphyritic. The porphyritic variety contains orthoclase and plagioclase phenocrysts. The non-porphyritic variety varies from medium- to coarse-grained; some samples are weakly foliated. The Klip Koppies granite is a poorly foliated, dark grey to dark porphyritic

granite with large orthoclase and plagioclase phenocrysts (Fig. 3i). The Straussburg granite, which is medium- to coarse-grained and locally porphyritic (Fig. 3k), with quartz commonly blue opaline. Where porphyritic it has large perthitic orthoclase phenocrysts and smaller quartz and plagioclase phenocrysts. The Friersdale charnockite is medium- to coarse-grained and has large plagioclase and orthoclase phenocrysts (Fig. 3l). It is characterised by blue opalescent quartz.

The majority of the granites are porphyritic and medium- to coarse-grained, with quartz primarily constituting the matrix ranging in size from 0.01 to 0.04 mm, commonly accompanied by plagioclase and/or orthoclase of similar grain size in smaller quantities. The constituent minerals of the groundmass are commonly sub-rounded/subhedral-anhedral. Quartz not only occurs as a constituent of the matrix, but commonly also as large individual grains, with grains as large as 3 mm present. K-feldspar phenocrysts, both orthoclase and microcline, and commonly perthitic (20%–33% of the phenocrysts) are common (with grain sizes up to 7 mm). Plagioclase phenocrysts, reaching sizes up to 5 mm, are also present. Phenocrysts throughout the suite typically exhibit euhedral to subhedral shapes. The non-porphyritic granites are divided into either medium-grained equigranular or inequigranular medium- to coarse-grained. Biotite commonly occurs in large aggregates which can reach up to 2.5 cm in size. Hematite and magnetite are common throughout the suite as accessory minerals (Bailie et al., 2017, 2011a; Cornell et al., 2012; Pettersson, 2008; Moen, 2007).

4 WHOLE-ROCK CHEMISTRY

4.1 Major-, Minor- and Trace-Element Chemistry

4.1.1 Keimoes Suite

A total of 31 samples of the Keimoes Suite were analysed (Tables 1, 2). The overwhelming majority of the samples are monzogranites, with a few granodiorites (Fig. 4). They range from

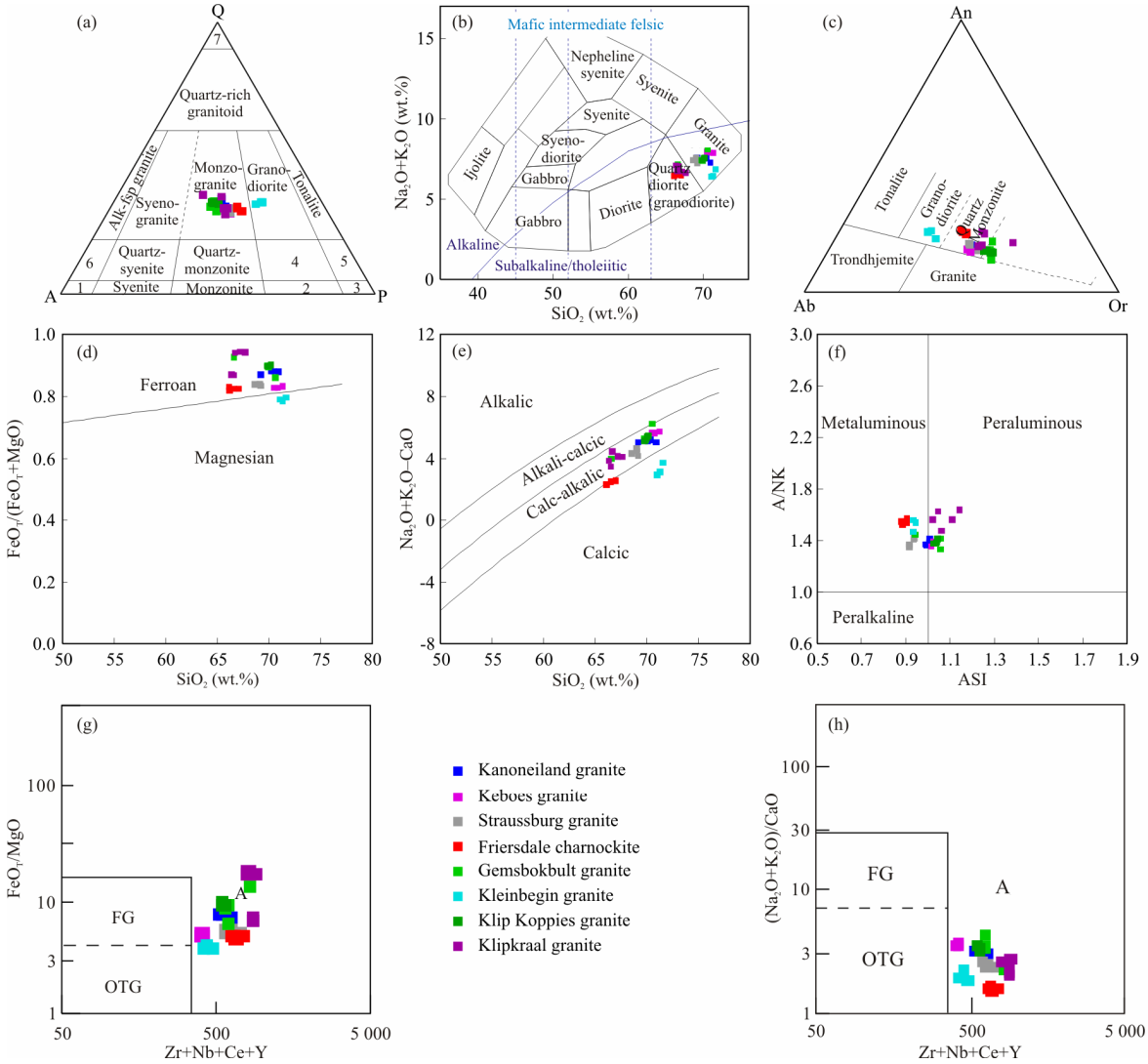

Figure 4. General geochemical characteristics and classification of the eastern Namaqua metamorphic province Keimoes Suite granites. (a) The QAP plot of Le Maitre et al. (1989); 1. alkali-feldspar syenite; 2. monzodiorite, monzogabbro; 3. diorite, gabbro; 4. q-monzodiorite, q-monzogabbro; 5. q-diorite, q-gabbro, q-anorthosite; 6. q-alk-fsp syenite; 7. quartzolite; (b) the total alkalis vs. silica (TAS) plot of Cox et al. (1979); (c) the An-Ab-Or ternary plot (after O'Connor, 1965); (d) $FeO_T/(FeO_T+MgO)$ vs. SiO_2 plot (after Frost et al., 2001); (e) the Na_2O+K_2O–CaO vs. SiO_2 plot (after Frost et al., 2001); (f) the molar $Al_2O_3/(Na_2O+K_2O)$ (A/NK) vs. aluminium saturation index (ASI) plot of Frost et al. (2001); (g) the FeO_T/MgO vs. Zr+Nb+Ce+Y plot of Whalen et al. (1987); (h) the $(Na_2O+K_2O)/CaO$ vs. Zr+Nb+Ce+Y plot of Whalen et al. (1987).

Table 1 Whole-rock major and minor element concentrations (wt.%) for the Keimoes Suite granitoids in the eastern NMP

Sample	Granite	SiO_2	TiO_2	Al_2O_3	FeO	MgO	CaO	Na_2O	K_2O	MnO	P_2O_5	Fe+Mg	ASI
Mka 1	Kanoneiland granite	70.91	0.76	12.85	4.92	0.67	2.24	2.49	4.78	0.12	0.25	0.085 0	0.99
Mka 3	Kanoneiland granite	70.41	0.71	13.33	4.66	0.62	2.35	2.74	4.82	0.11	0.25	0.080 4	0.97
Mka 6	Kanoneiland granite	69.16	0.74	13.91	4.97	0.73	2.53	2.84	4.75	0.11	0.26	0.087 3	0.99
Mka 7	Kanoneiland granite	70.14	0.77	13.26	4.90	0.66	2.39	2.70	4.81	0.11	0.26	0.084 6	0.97
Mkb 1	Keboes granite	71.27	0.49	13.84	3.44	0.69	2.13	2.97	4.89	0.08	0.18	0.065 1	1.00
Mkb 2	Keboes granite	70.79	0.50	14.23	3.37	0.70	2.25	3.02	4.87	0.08	0.18	0.064 2	1.01
Mkb 6	Keboes granite	70.50	0.50	14.43	3.37	0.70	2.29	3.09	4.86	0.08	0.18	0.064 2	1.01
Ms 1	Straussburg granite	68.58	0.97	13.55	5.04	0.96	3.07	2.81	4.60	0.12	0.30	0.093 9	0.91
Ms 2	Straussburg granite	69.11	0.96	13.17	4.93	0.94	3.00	2.62	4.87	0.12	0.28	0.091 8	0.90
Ms 6	Straussburg granite	69.16	0.92	13.31	4.95	0.98	3.05	2.76	4.45	0.12	0.30	0.093 2	0.91
Ms 7	Straussburg granite	69.02	1.01	13.14	4.99	0.94	2.93	2.65	4.92	0.12	0.28	0.092 8	0.89
Mf 1	Friersdale charnockite	67.02	1.25	12.96	6.43	1.37	3.89	2.52	3.94	0.15	0.48	0.123 4	0.87
Mf 4	Friersdale charnockite	66.13	1.28	13.15	6.63	1.47	4.21	2.62	3.85	0.16	0.50	0.128 7	0.85
Mf 6	Friersdale charnockite	66.09	1.31	13.30	6.71	1.36	4.11	2.65	3.79	0.16	0.51	0.127 3	0.87
Mf 7	Friersdale charnockite	66.53	1.29	12.89	6.73	1.42	4.00	2.55	3.94	0.16	0.49	0.128 8	0.85
Mge 1	Gemsbokbult granite	70.57	0.72	13.59	4.12	0.66	1.86	2.51	5.58	0.09	0.29	0.073 7	1.03
Mge 2	Gemsbokbult granite	69.77	0.83	13.22	5.54	0.61	2.17	2.28	5.14	0.13	0.32	0.092 2	1.03
Mge 3	Gemsbokbult granite	69.93	0.77	13.13	5.46	0.65	2.23	2.30	5.09	0.12	0.32	0.092 1	1.01
Mge 5	Gemsbokbult granite	66.58	1.03	12.98	7.79	0.61	3.21	2.14	5.03	0.19	0.43	0.123 5	0.91
Mkle 1	Kleinbegin granite	71.61	0.48	13.80	3.18	0.81	3.11	3.51	3.33	0.08	0.11	0.064 2	0.93
Mkle 2	Kleinbegin granite	71.02	0.56	13.80	3.61	0.96	3.45	3.42	2.97	0.09	0.13	0.074 1	0.92
Mkle 3	Kleinbegin granite	71.30	0.54	13.83	3.46	0.94	3.29	3.54	2.90	0.08	0.12	0.071 6	0.93
Mks 1	Klip Koppies granite	70.02	0.76	13.11	5.39	0.59	2.14	2.28	5.27	0.13	0.31	0.089 6	1.01
Mks 2	Klip Koppies granite	70.16	0.75	13.15	5.22	0.56	2.14	2.35	5.23	0.12	0.30	0.086 7	1.01
Mks 3	Klip Koppies granite	69.81	0.81	13.28	5.37	0.61	2.27	2.39	5.01	0.12	0.32	0.089 9	1.01
Mks 4	Klip Koppies granite	70.05	0.81	13.21	5.16	0.57	2.23	2.50	5.04	0.12	0.31	0.086 0	1.00
MkI 2	Klipkraal granite	67.19	0.92	13.33	8.12	0.47	2.58	1.54	5.17	0.21	0.48	0.124 8	1.09
MkI 4	Klipkraal granite	67.66	0.95	13.15	7.96	0.49	2.52	2.22	4.39	0.18	0.48	0.122 9	1.09
MkI 5	Klipkraal granite	66.34	1.12	14.03	6.61	0.98	3.23	2.29	4.80	0.15	0.46	0.116 3	0.98
MkI 6	Klipkraal granite	66.53	1.16	13.89	6.81	1.02	3.24	2.23	4.50	0.15	0.47	0.120 0	1.00
Mkl 3	Klipkraal granite	66.68	0.97	13.34	8.17	0.50	2.60	2.46	4.60	0.19	0.49	0.126 2	1.01

metaluminous to weakly peraluminous. They are dominantly ferroan, except for the Kleinbegin granite, and calc-alkalic, except for the Kleinbegin granite and Friersdale charnockite, the latter nominally calcic, and plot mainly within the A-type field on A-type discrimination diagrams (Fig. 4).

The SiO_2 values range between 66.09 wt.% and 71.61 wt.%, with FeO_T covering a large range between 3.18 wt.% and 8.17 wt.%. The Friersdale charnockite has the highest TiO_2, MgO and CaO, and the lowest SiO_2 concentrations, whereas the Kleinbegin granite has the highest SiO_2, and lowest TiO_2 and FeO_T concentrations. The Klip Koppies and Kleinbegin granites have low concentrations of both MgO and CaO, and elevated Na_2O contents. The granitoids are enriched in Ti, Fe, Mn, P and K, and depleted in Al and Na relative to average granites and granodiorites. In Harker plots (using element concentrations instead of oxides), for many of the granites, Si shows negative correlations with Fe, Mg, Ti, Ca, P and the aluminium saturation index (ASI) (Al/(Ca–1.67P+Na+K)), and broadly positive correlations for Al, K and Na (ESM2, Fig. S1).

The oldest granite, the Keboes granite, is the most highly fractionated. By contrast, the youngest member, the Friersdale charnockite, is the least SiO_2-rich, and the least fractionated, in terms of REE and trace element contents, and also has the highest HFSE content.

Principal component analysis (PCA) (ESM2, Fig. S2) shows that each granite is distinctly different, forming its own separate cluster, and therefore indicating that each granite is genetically unrelated to the others, coming from different sources. The more fractionated plutons (Kanoneiland, Keboes, Gemsbokbult, Kleinbegin and Klip Koppies granites) show trends parallel to the major component (SiO_2), indicating that this played the major role in their compositional diversity, whereas the compositions of the less fractionated, and more mafic granites (Friersdale charnockite and Klipkraal granite)

Table 2 Whole-rock trace element concentrations (ppm) for the Keimoes Suite granitoids in the eastern NMP

Rock type	Kanoneiland granite				Keboes granite			Straussburg granite				Friersdale charnockite			
Sample	Mka 1	Mka 3	Mka 6	Mka 7	Mkb 1	Mkb 2	Mkb 6	Ms 1	Ms 2	Ms 6	Ms 7	Mf 1	Mf 4	Mf 6	Mf 7
Large ion lithophile elements (LILEs)															
Cs	14.25	12.64	11.56	11.28	10.97	10.70	12.35	6.25	5.64	5.31	13.19	5.27	5.28	5.87	6.82
Rb	245.90	234.50	233.15	227.81	255.71	242.89	185.62	195.89	224.48	199.24	278.56	156.57	161.38	159.36	167.78
Ba	873.99	882.11	823.74	869.53	715.25	714.42	255.33	1 103.89	1 076.45	1 193.40	883.65	1 133.75	1 129.59	1 069.73	1 105.29
Sr	159.63	148.32	142.92	155.34	130.96	130.74	294.31	187.98	171.47	197.30	126.64	279.40	277.26	264.33	240.02
Pb	32.62	31.97	34.80	31.04	32.49	30.95	18.02	30.78	32.41	37.09	40.57	29.29	27.33	28.80	27.95
High field strength elements (HFSEs)															
Th	22.42	21.50	34.69	22.56	34.41	34.47	14.47	25.02	34.12	57.78	53.78	17.12	17.07	20.08	17.45
U	3.8	2.5	4.0	4.5	7.2	7.6	3.5	4.0	4.4	4.9	6.6	3.7	3.2	4.3	5.9
Zr	350	298	332	337	229	235	308	413	432	411	334	395	422	387	504
Hf	10.0	8.4	9.5	9.5	6.6	6.8	7.3	11.2	12.0	11.0	9.8	10.3	11.1	10.3	13.5
Nb	22.4	22.7	21.2	21.2	17.3	16.4	16.4	20.6	22.3	22.9	19.0	22.2	24.9	24.4	27.6
Ta	2.1	2.6	1.9	1.6	3.0	1.5	1.7	1.5	2.7	1.6	2.0	1.5	1.8	2.4	2.6
Y	56.2	73.1	69.6	46.7	41.0	40.9	21.1	48.2	50.3	53.2	50.9	63.1	59.7	59.1	59.9
Transition elements															
Sc	17.5	16.3	20.1	14.3	12.3	12.1	11.8	16.6	16.1	19.0	11.9	22.8	21.9	21.3	20.9
Cr	155	67	82	116	131	79	102	143	163	69	182	53	80	162	74
Ni	9.8	12.4	9.7	10.1	11.5	11.7	10.3	12.9	14.8	18.1	13.9	16.1	15.1	18.8	18.6
Co	7.5	7.0	8.0	7.1	5.9	6.0	8.2	9.4	9.2	10.9	6.8	13.6	12.8	13.3	15.6
V	61.1	52.6	60.3	58.2	50.4	47.4	79.1	87.5	90.5	91.6	66.8	115.3	115.0	125.9	117.0
Zn	97.3	93.2	98.7	90.7	71.7	77.8	129.5	75.6	77.9	90.2	76.7	110.5	99.7	104.8	108.8
Cu	11.7	21.5	14.6	12.2	14.0	20.6	43.2	14.5	26.3	31.4	13.4	67.7	16.0	100.3	28.9
Rare earth elements (REEs)															
La	65.4	63.0	98.3	67.7	57.3	56.4	32.6	73.2	67.7	120.0	85.7	85.4	82.2	81.6	75.1
Ce	139.1	131.1	215.5	142.4	124.7	122.7	57.1	148.5	144.4	249.9	189.4	180.2	174.7	174.2	160.3
Pr	16.4	15.5	25.2	16.5	15.0	14.4	5.9	16.9	17.1	27.6	20.8	21.3	20.7	20.4	19.4
Nd	62.9	57.8	95.2	63.3	56.9	56.1	21.1	61.8	64.7	96.3	76.1	82.4	81.0	79.8	74.5
Sm	12.7	12.4	18.0	12.0	11.0	10.9	4.3	11.3	12.1	15.8	13.7	15.6	15.5	14.5	14.8
Eu	2.04	2.12	2.05	2.02	1.40	1.28	0.88	2.04	2.05	2.35	1.60	3.11	3.05	2.86	2.81
Gd	10.83	10.88	14.47	9.46	8.43	8.36	3.41	9.14	9.56	11.92	10.54	13.73	12.62	12.22	12.45
Tb	1.69	1.92	2.23	1.44	1.30	1.25	0.57	1.42	1.54	1.72	1.55	2.02	1.86	1.86	1.82
Dy	10.54	12.89	13.61	8.76	7.63	7.46	3.35	8.87	9.58	10.23	8.91	12.16	11.09	11.15	11.23
Ho	2.06	2.67	2.63	1.72	1.56	1.48	0.71	1.80	1.92	1.95	1.75	2.40	2.36	2.25	2.31
Er	6.09	7.99	7.59	4.89	4.22	4.52	2.25	5.12	5.56	5.43	5.24	6.59	6.67	6.51	6.19
Tm	0.83	1.27	1.09	0.73	0.62	0.60	0.34	0.79	0.77	0.92	0.77	0.95	0.88	0.94	0.95
Yb	6.09	8.62	7.29	4.91	4.25	4.31	2.11	5.10	5.46	5.57	5.56	6.60	6.02	6.21	6.24
Lu	0.85	1.15	1.02	0.65	0.63	0.59	0.25	0.75	0.80	0.86	0.79	0.96	0.88	0.87	0.86

Table 2 Continued

Rock type	Gemsbokbult granite				Kleinbegin granite			Klip Koppies granite				Klipkraal granite				
Sample	Mge 1	Mge 2	Mge 3	Mge 5	Mkle 1	Mkle 2	Mkle 3	Mks 1	Mks 2	Mks 3	Mks 4	MkI 2	MkI 4	MkI 5	MkI 6	Mkl 3
Large ion lithophile elements (LILEs)																
Cs	13.86	3.51	3.40	2.45	1.85	1.99	2.57	5.73	6.48	6.05	6.02	2.51	4.57	2.46	2.07	7.22
Rb	292.22	209.68	193.08	189.15	107	99	106	197	206	200	197	174	204	200	186	220
Ba	930.60	1 115.39	1 102.02	1 369.03	1 135	982	959	1 043	1 084	1 050	1 061	1 443	1 467	1 198	1 186	1 588
Sr	133.19	165.49	151.13	167.43	154	157	156	142	143	148	145	151	147	165	171	165
Pb	39.25	36.89	35.25	39.36	18.9	17.7	16.2	34.2	37.5	35.0	34.4	41.3	40.9	41.7	39.3	38.6
High field strength elements (HFSEs)																
Th	55.47	28.98	28.91	37.46	16.9	13.1	5.9	27.3	29.1	28.9	28.1	36.0	41.8	54.6	51.1	38.3
U	6.6	3.0	2.3	3.6	2.0	1.6	1.5	3.2	3.2	3.2	2.7	3.6	3.5	4.5	4.4	4.1
Zr	342	369	351	510	275	307	308	324	326	340	344	483	419	515	524	535
Hf	10.1	10.3	9.9	14.1	7.9	8.0	8.4	9.2	9.3	9.5	9.6	13.7	12.2	14.4	14.2	14.6
Nb	20.1	20.9	21.6	28.8	11.4	13.3	10.9	20.4	19.9	21.3	21.2	24.4	23.6	27.3	28.5	29.6
Ta	2.0	1.4	2.9	3.5	0.8	3.0	3.0	1.9	1.3	2.2	1.3	2.5	2.9	1.5	3.1	3.8
Y	54.1	52.7	50.3	77.3	59.6	56.7	44.0	49.7	52.3	51.3	50.4	92.5	92.6	69.2	69.0	99.7
Transition elements																
Sc	12.2	19.2	19.7	24.5	10.0	12.6	10.8	17.8	18.1	18.1	18.1	23.3	25.3	20.9	21.5	26.7
Cr	243	91	161	133	98.9	167.2	184.0	113.3	72.5	147.4	93.2	101.8	72.3	50.7	84.1	149.6
Ni	14.4	10.5	12.0	11.4	15.8	22.9	21.2	11.4	22.9	12.2	9.0	7.1	7.4	11.1	11.5	11.7
Co	6.9	6.7	7.1	8.2	8.1	9.6	9.0	6.5	6.7	6.8	6.5	7.8	7.9	11.7	11.4	9.1
V	71.8	47.4	53.0	37.6	61.1	77.4	73.6	46.1	42.4	49.6	45.8	30.0	26.2	72.9	80.0	35.1
Zn	74.8	102.4	103.5	139.0	45.8	53.3	47.5	97.6	101.5	96.1	100.8	122.6	124.8	113.9	107.1	146.1
Cu	21.4	14.3	17.2	32.6	37.6	76.5	43.2	17.7	38.8	17.9	13.5	20.2	18.5	25.1	26.7	27.6
Rare earth elements (REEs)																
La	91.0	78.4	77.1	99.3	40.7	43.8	24.7	73.6	73.9	76.4	73.3	103.8	120.8	119.1	115.4	113.0
Ce	198.8	168.2	165.1	221.4	96.2	98.1	56.6	157.4	154.4	162.5	156.9	223.3	255.0	270.3	260.9	241.5
Pr	21.9	19.8	19.4	26.6	12.0	12.1	7.4	18.7	18.5	19.2	18.4	26.6	30.5	33.1	32.0	29.1
Nd	80.8	77.1	75.6	107.3	46.4	46.2	31.6	71.4	73.0	75.2	71.8	104.6	118.9	129.5	128.5	115.4
Sm	14.4	15.0	14.7	20.3	9.78	9.05	6.99	14.17	14.49	14.95	14.12	20.62	23.20	23.56	22.72	21.73
Eu	1.79	2.40	2.23	3.08	1.33	1.48	1.24	2.11	2.20	2.25	2.22	3.07	3.37	2.79	2.71	3.49
Gd	10.82	12.44	11.49	16.51	9.28	8.70	6.68	11.54	11.89	11.89	11.97	17.96	19.40	16.88	16.34	19.64
Tb	1.62	1.77	1.64	2.44	1.60	1.47	1.16	1.71	1.65	1.68	1.65	2.74	2.91	2.24	2.26	3.06
Dy	9.54	10.05	9.68	14.73	10.35	9.20	7.31	9.32	9.96	9.57	9.79	16.71	17.69	13.41	13.25	18.93
Ho	1.98	1.93	1.94	2.96	2.22	1.94	1.57	1.87	1.97	1.87	1.90	3.49	3.61	2.66	2.67	3.72
Er	5.56	5.61	5.27	8.53	6.18	5.77	4.59	5.17	5.49	5.43	5.54	10.26	9.94	7.24	7.39	10.81
Tm	0.80	0.77	0.77	1.18	0.85	0.90	0.66	0.73	0.75	0.73	0.78	1.40	1.46	1.06	0.95	1.66
Yb	5.72	5.42	5.18	8.05	5.59	5.86	4.61	4.99	5.13	4.87	5.12	9.85	9.32	6.83	6.82	10.57
Lu	0.88	0.77	0.74	1.16	0.76	0.88	0.71	0.70	0.72	0.70	0.75	1.40	1.32	0.85	0.98	1.55

are dominantly controlled by CaO and FeO_T, respectively, showing trends parallel to these factors (ESM2, Fig. S2). The Straussburg granite falls between these two clusters. K_2O has controlled some compositional variation in the Klip Koppies, Gemsbokbult and Kanoneiland granites, and Na_2O in the Kleinbegin granite.

Ti, Ca and P (along with A/CNK (molar $Al_2O_3/(CaO+Na_2O+K_2O)$ and ASI show positive, and Si, K, Na, Al and $Mg^{\#}$ show negative correlations with maficity (molar Fe+Mg) (Fig. 5) (as described for granitic suites, e.g., Clemens et al., 2011). The granitoids with the highest maficity are the Klipkraal granite and the Friersdale charnockite. They also have the highest Fe, Mg, Ti and P, and lowest Si contents of all the granitoids. By contrast, the Kleinbegin and Keboes granites have the lowest maficities and lowest Fe, Ti, and P, and highest Si and Na contents; the Kleinbegin granite has the lowest K contents of the granitoids.

Relative to the primitive mantle (PM) values of Sun and McDonough (1989), the granites are enriched in the large ion lithophile elements (LILE) (Cs, Rb, Ba) relative to the high field strength elements (HFSE) (the rare earth elements (REE), Y, Zr, Hf, Nb, Ta, Ti) (Fig. 6). Overall, there are noticeable depletions in Ba, Nb, Sr, P, Eu and Ti, with mild depletions in Rb, K and Zr (slight), and with enrichments in Th, U, Pb and the LREE (La, Ce, Pr, Nd, Sm). The enrichments emphasise an upper crustal component to the granites due to the fact that these elements are particularly enriched in that portion of the continental crust (cf. avg. crust-normalized plot, Fig. 6). The Nb-Ta depletion suggests subduction-influenced processes. In the average crust-normalized plot, the HREE (Tb, Tm and Yb, along with Y) are enriched relative to the LREE, but there are similar depletions in Ba, K, Sr, P, Zr (slight), and Ti.

The REE plot (normalised to the PM values of McDonough and Sun, 1995) show enrichment of the LREE relative to the HREE [$(La/Yb)_{PM}$=3.63–14.61], and negative europium anomalies [$(Eu/Eu^*)_{PM}$=0.39–0.70]. The LREE are moderately fractionated [$(La/Sm)_{PM}$: 2.22–4.78], whereas the HREE show relatively flat patterns [$(Gd/Yb)_{PM}$: 1.02–1.99].

4.1.2 Koras Group

A total of 30 samples of the Koras Group were analysed, of which 16 are rhyolitic porphyries from both successions (Tables 3, 4). This review will focus predominantly on the rhyolites. These have characteristic rhyolitic compositions (Figs. 7a–7c). The majority of the rhyolite samples are metaluminous, with only a few being peralkaline (predominantly those of the Swartkopsleegte Formation of the lower succession), and are mostly alkali-calcic and magnesian (Figs. 7d–7f).

The Koras Group rhyolites have higher FeO, MgO, CaO, Na_2O, K_2O, TiO_2, and MnO, and lower SiO_2 and Al_2O_3 relative to average rhyolite. All the major elements, except for K_2O, show negative trends relative to SiO_2 (ESM2, Fig. S3). Na_2O concentrations, when taken with those of the basaltic andesites, display a two-step trend or pattern, with increasing trends from the basaltic andesites up to intermediate compositions and decreasing trends for the higher SiO_2 compositions of the rhyolites. Sr follows a similar two-step trend as Na_2O, while Ba follows the K_2O trend. The abundances of incompatible elements, such as Rb, Nb, Zr, Th, and U are positively correlated with SiO_2 content, whereas the negative trends of compatible elements (Ni, Cr and V) with increasing SiO_2 correspond with similar trends of MgO and Fe_2O_3 with differentiation (Bailie et al., 2012).

In terms of PCA, the lower succession rhyolitic porphyries show patterns or trends suggesting that Na and Ca are the main compositional variable, with the limited number of samples precluding any in-depth interpretation, whereas for the upper succession, Si and K play important roles (ESM2, Fig. S4). The lower succession forms separate trends on most of the correlation plots (ESM2, Fig. S5), suggesting that it possibly formed along its own separate evolutionary path relative to the upper succession. On maficity plots (Fig. 5), the Koras Group rhyolites show separate trends to those of the Keimoes Suite granitoids. Positive trends against maficity are present for Ti, Ca, and Al, and negative trends for Si and K; Na, P, $Mg^{\#}$, A/CNK and ASI have vertical to no proper trends.

On PM-normalized multi-element trace-element plots (spider diagrams), there are no apparent distinctions between the lower and upper successions (Fig. 8). Relative to the primitive mantle, the rhyolitic porphyries are enriched in the LIL elements relative to the HFS elements (Fig. 8). There are depletions in Ba, Nb, Ta, K, Zr, Hf (slight), Sr, P and Ti (the latter three strongly, with enrichments in Th, U and Pb. The LREE are enriched relative to the HREE, the latter having a flat pattern. Nb is depleted relative to the other HFSE, but Th is enriched relative to both Nb and Ta, as well as the HREE (Bailie et al., 2012). Average crust-normalized patterns show similar enrichments and depletions to the PM-normalized plot, apart from a HREE enrichment relative to the LREE (Fig. 8).

The PM-normalized REE plot (Fig. 8) shows a slightly negative sloping trend, with a slight enrichment of the LREE relative to the HREE [$(La/Yb)_{PM}$: 7.10–14.39], moderate fractionation in the LREE [$(La/Sm)_{PM}$: 3.28–4.95], relatively flat HREE patterns [$(Gd/Yb)_{PM}$: 1.11–1.71], and slight negative europium anomalies [$(Eu/Eu^*)_{PM}$: 0.57–0.66]. The Swartkopsleegte Formation of the lower succession has a much smaller range in terms of ratios (but also fewer samples), and shows a shallower LREE slope, and overall LREE/HREE enrichment, and flatter overall HREE slope compared to the rhyolites of the upper succession.

4.2 Isotope Geochemistry

The Keimoes Suite granitoids have $^{143}Nd/^{144}Nd$ ratios for time of emplacement which vary between 0.510 78 and 0.511 35 (Table 5). The $\varepsilon_{Nd}(t)$ values, calculated relative to each granite's emplacement age, fall within a range from 2.78 to -2.95, with the Kleinbegin granite samples having the most negative values (-4.87 to -8.58) (Fig. 9). The Kanoneiland granite is the only granite with mostly positive $\varepsilon_{Nd}(t)$ values (0.65 to 2.78), apart from one sample of the Friersdale charnockite, with the vast majority of the $\varepsilon_{Nd}(t)$ values being negative, suggesting weakly to mildly enriched sources, with a strongly enriched crustal source for the Kleinbegin granite. Sm-Nd model ages (T_{DM}) vary from 1.62–1.99 Ga, with the Kleinbegin granite having older model ages of 1.91–2.55 Ga, and a younger model age of 1.40 Ga for Kanoneiland granite sample Kan1. Initial $^{87}Sr/^{86}Sr$ ratios

Table 3 Whole-rock major and minor element concentrations (wt.%) for the Koras Group bimodal volcanic rocks in the western Kheis terrane

Sample	Rock type	Succession	SiO_2	TiO_2	Al_2O_3	FeO	MgO	CaO	Na_2O	K_2O	MnO	P_2O_5	Fe+Mg	ASI
K1	Boom River basaltic andesites	Lower	55.25	1.09	14.80	9.41	5.49	9.27	2.14	1.31	0.15	0.14	0.267 2	0.68
K2	Boom River basaltic andesites	Lower	53.76	1.10	15.42	9.48	5.61	11.40	1.98	0.96	0.16	0.13	0.271 2	0.62
K11	Boom River basaltic andesites	Lower	57.41	1.23	14.75	9.86	4.66	7.21	2.65	1.92	0.16	0.16	0.252 7	0.76
K14	Boom River basaltic andesites	Lower	54.82	1.13	15.11	9.85	5.73	9.16	2.98	0.90	0.18	0.14	0.279 4	0.68
K15	Boom River basaltic andesites	Lower	56.06	1.16	15.14	10.07	6.09	6.23	2.71	2.17	0.18	0.20	0.291 2	0.85
K16	Boom River basaltic andesites	Lower	56.42	1.12	14.68	5.02	1.70	9.53	10.05	0.18	1.18	0.15	0.111 9	0.43
K17	Boom River basaltic andesites	Lower	54.62	1.12	15.24	10.16	5.81	8.48	2.31	1.96	0.17	0.13	0.285 7	0.72
K25	Boom River basaltic andesites	Lower	58.73	0.98	14.12	8.89	5.19	10.08	0.65	1.08	0.15	0.13	0.252 5	0.69
W28	Boom River basaltic andesites	Lower	55.43	1.25	15.07	9.96	5.23	8.99	2.18	1.57	0.16	0.16	0.268 4	0.70
W29	Boom River basaltic andesites	Lower	55.61	1.28	14.85	10.01	5.15	8.90	2.24	1.62	0.16	0.16	0.267 2	0.69
K3	Leeuwdraai rhyolitic porphyry	Upper	71.34	0.70	13.30	2.74	0.76	1.78	3.93	5.19	0.18	0.07	0.057 1	0.87
K3b	Leeuwdraai rhyolitic porphyry	Upper	73.18	0.73	13.01	2.00	0.73	1.09	3.28	5.73	0.19	0.04	0.046 1	0.96
K4	Leeuwdraai rhyolitic porphyry	Upper	73.82	0.62	12.20	2.20	0.62	1.29	3.64	5.38	0.17	0.07	0.045 9	0.87
K8	Swartkopsleegte rhyolitic porphyry	Lower	70.94	0.96	13.04	2.44	1.04	1.88	4.59	4.70	0.34	0.07	0.059 7	0.82
K9	Swartkopsleegte rhyolitic porphyry	Lower	71.59	0.91	12.63	1.86	0.53	2.59	5.66	3.80	0.34	0.09	0.039 0	0.70
K12	Leeuwdraai rhyolitic porphyry	Upper	72.16	0.70	13.04	2.28	0.73	1.85	3.51	5.47	0.18	0.07	0.049 8	0.87
K13	Leeuwdraai rhyolitic porphyry	Upper	72.26	0.75	12.70	2.06	0.62	1.86	4.21	5.26	0.20	0.08	0.044 0	0.80
K19	Swartkopsleegte rhyolitic porphyry	Lower	70.95	0.91	12.92	1.77	0.90	2.04	4.80	5.26	0.34	0.10	0.047 1	0.75
K21	Leeuwdraai rhyolitic porphyry	Upper	72.32	0.84	11.98	2.74	0.70	1.66	4.20	5.21	0.27	0.07	0.055 5	0.77
K22	Leeuwdraai rhyolitic porphyry	Upper	72.58	0.70	12.74	2.28	0.49	1.88	3.46	5.62	0.18	0.05	0.043 9	0.84
K23	Leeuwdraai rhyolitic porphyry	Upper	72.04	0.73	13.02	2.33	0.69	1.94	3.58	5.44	0.19	0.05	0.049 5	0.85
K24	Leeuwdraai rhyolitic porphyry	Upper	73.09	0.65	13.19	2.10	0.49	1.51	2.82	5.92	0.19	0.04	0.041 3	0.96
K33	Rouxville rhyolitic porphyry	Upper	72.23	0.77	13.12	2.46	0.67	1.47	3.76	5.27	0.19	0.05	0.050 9	0.90
K35	Welgevind rhyolitic porphyry	Upper	68.64	0.98	13.98	3.01	1.24	2.38	5.20	4.14	0.31	0.12	0.072 7	0.81
K36	Welgevind rhyolitic porphyry	Upper	70.40	0.84	13.91	2.87	1.12	1.65	3.75	5.13	0.26	0.07	0.067 7	0.95
K37	Welgevind rhyolitic porphyry	Upper	71.22	0.81	13.79	2.74	0.87	2.08	3.24	4.96	0.23	0.05	0.059 8	0.96

Table 4 Whole-rock trace element concentrations (ppm) for the Koras Group bimodal volcanic rocks in the western Kheis terrane (lower succession)

Formation	Boom River										Swartkopsleegte		
Rock type	Basaltic andesites										Rhyolitic porphyry		
Sample	K1	K2	K11	K14	K15	K16	K17	K25	W28	W29	K8	K9	K19
Large ion lithophile elements (LILE)													
Cs	1.8	1.3	2.6	2.1	1.9	0.9	1.8	1.1	0.8	1.3	2.1	2.5	3.6
Rb	53.4	41.7	70.8	45.3	70.7	50.2	65.8	44.4	52	63.5	198	203	220
Ba	354	286	727	320	750	373	452	244	383	415	1 152	1 131	1 214
Sr	214	166	307	296	352	393	218	210	207	230	186	184	173
Pb	11	14	7	11	8	24	9	10	10	12	21	12	18
High field strength elements (HFSE)													
Th	7	6.7	7.8	7.3	6.7	6.3	6.7	6.1	7.2	8	23.2	24.4	22
U	1.5	1.5	1.7	1.6	1.5	1.3	1.5	0.3	1.8	1.9	5.5	5.4	5.1
Zr	120	118	123	129	115	84	118	107	127	141	348	356	322
Hf	4	4	4.2	4.6	4.1	3.1	4.3	3.8	4.4	4.7	11.4	11.4	10.4
Nb	8.4	8.3	9.8	9.7	8.5	7.8	8.7	7.8	10	10.9	26.9	26.4	26.2
Ta	0.5	0.6	0.7	0.6	0.6	0.5	0.6	0.5	0.6	0.7	1.7	1.9	1.7
Y	26.2	26	28.5	27.7	25.9	24.6	25.9	24.3	26.4	28.6	66.5	66.1	62.6
Transition elements													
Sc	25.5	23.7	26.5	30	30.5	29.4	29.6	24.7	25.8	26.3	15.6	15.5	14.8
Cr	132	121	51	139	137	131	134	190	91	93	8	6	8
Ni	61	64	50	61	59	60	61	51	68	65	5	3	3
Co	45	45	38	42	43	44	41	38	44	46	6	7	6
V	242	230	238	226	244	221	237	204	237	225	45	40	36
Zn	95	91	102	106	100	98	101	86	96	108	119	120	121
Cu	104	106	99	116	107	114	95	62	109	241	81	4	5
Ga	18.9	19.7	17.6	17.7	17.3	18.7	19.2	19.5	18.8	20.1	21.1	21.2	19.8
Rare earth elements (REEs)													
La	21	21	28	26	24	24	24	21	23	25	86	89	80
Ce	48.8	47.4	61.3	55.5	51.7	51.8	53.2	45.8	50.4	56.2	197.4	201.5	185
Pr	5.4	5.2	6.5	6.1	5.5	5.4	5.6	4.9	5.6	6.3	20.6	21	19.7
Nd	22.1	21.8	27.6	25.9	24.3	23.7	24.8	21.6	23.4	25.3	86	89.4	82.1
Sm	4.9	4.9	5.6	5.8	5.3	5	5.1	4.6	5.1	5.7	16	16.7	15.3
Eu	1.4	1.3	1.5	1.4	1.4	1.4	1.3	1.2	1.3	1.5	2.9	3.1	2.9
Gd	5	5.1	6.2	5.9	5.7	5.3	5.3	4.6	5.3	5.6	15.1	14.5	13.4
Tb	0.9	0.9	1.1	1.1	1	1	1	0.9	0.9	1	2.5	2.7	2.4
Dy	5	5.1	6.3	5.6	5.6	5.3	5.7	4.9	5.1	5.4	14.2	14.4	12.9
Ho	1	1.1	1.2	1.1	1.1	1	1.1	1	1.1	1.2	2.6	2.7	2.5
Er	4	4	3.3	3.3	3.1	2.8	3.1	2.8	3.9	4.2	7.5	7.8	6.8
Tm	0.4	0.5	0.5	0.5	0.5	0.4	0.5	0.4	0.4	0.5	1.1	1.2	1
Yb	3.7	3.6	3.7	3.6	3.3	3.2	3.5	3.1	3.7	3.9	8	8.5	7.4
Lu	0.4	0.4	0.4	0.5	0.4	0.3	0.4	1.4	0.4	0.5	1	1.1	0.9

Table 4 Continued (upper succession)

Formation	Leeuwdraai									Welgevind			Rouxville
Rock type	Rhyolitic porphyry									Rhyolitic porphyry			Rhyolitic porphyry
Sample	K3	K3b	K4	K12	K13	K21	K22	K23	K24	K35	K36	K37	K33
Large ion lithophile elements (LILEs)													
Cs	1.8	2.3	1.7	2.2	2.6	2.4	0.9	3.1	3.3	0.9	2	2.4	2.3
Rb	194	241	219	201	206	236	231	219	231	125	194	190	211
Ba	1 173	1 832	1 857	1 490	1 605	1 541	1 552	1 521	1 682	1 639	2 016	1 895	1 661
Sr	129	142	131	180	150	226	162	170	148	426	247	232	140
Pb	34	38	38	43	39	45	37	38	34	19	37	26	39
High field strength elements (HFSEs)													
Th	29.6	41	37	35.2	35.7	36.4	33.4	33.3	33.1	34.7	35.1	37.1	34.6
U	3.9	5	4	4.9	4.8	5.2	4.2	4.6	4.3	3.9	4.6	4.8	4.5
Zr	169	220	184	177	191	202	165	168	186	236	178	184	191
Hf	6	7.9	7.2	6.5	7.2	7.5	6.2	6.3	7.1	8.3	7.1	6.9	7
Nb	27.6	31.6	27.2	25.7	27.6	27.7	23.6	25.3	25.9	22.6	20.7	20	29
Ta	1.8	2.2	2	1.8	2	2	1.7	1.8	2	1.3	1.3	1.3	2
Y	56.1	73.5	60.9	61.9	60.8	64.2	60.7	62.4	60.2	51.7	52.3	51.5	63.5
Transition elements													
Sc	8	11.2	9.5	8.8	9.1	9.3	9.3	9.1	8.4	15.6	12.1	11.7	10.3
Cr	7	9	6	7	11	7	7	7	6	9	5	4	8
Ni	4	9	8	4	7	4	6	14	7	13	4	14	10
Co	6	9	6	6	7	6	6	6	5	12	5	5	6
V	36	40	34	36	38	37	33	35	25	77	38	38	35
Zn	65	93	68	76	77	63	64	67	67	106	83	83	73
Cu	9	4	8	8	15	10	8	9	9	17	47	8	4
Ga	15.9	18.5	16	18.4	16.6	16.8	17.4	17.6	15.5	19	19.5	19	17.7
Rare earth elements (REEs)													
La	85	127	86	115	114	108	113	112	106	118	138	139	117
Ce	192.7	255.8	216.3	237.6	236	241.8	236.8	229.1	206.1	261.2	297.7	298.9	232.9
Pr	19.3	25.5	19.6	22.6	22.4	22.1	22.4	22	20.2	25.3	29	30.1	23.7
Nd	69.7	100.1	78.5	87.4	86.8	87.1	87.1	86.4	78.8	104.9	117.9	118.2	89.5
Sm	12.3	16.3	14.1	14.8	14.8	15.1	14.9	14.2	13.7	18.1	18	18.5	15.3
Eu	2.1	3.1	2.7	2.8	2.8	2.7	2.7	2.8	2.5	3	3.4	3.4	2.7
Gd	10	14.2	11.8	13	13.4	12.8	12.2	12.5	12.3	13.3	13.8	13.3	13.6
Tb	1.9	2.6	2.2	2.3	2.5	2.4	2.4	2.3	2.2	2.3	2.3	2.4	2.5
Dy	10.3	14.7	12.5	12.9	13.4	13.8	12.7	13.2	12.8	11.7	11.7	12.3	13.6
Ho	2.1	2.8	2.5	2.5	2.6	2.7	2.5	2.5	2.5	2.2	2.1	2.2	2.7
Er	7.6	8.2	7.3	7.3	7.4	7.7	7.2	7.1	7.2	6	5.8	6.2	7.7
Tm	0.9	1.3	1.1	1.1	1.1	1.2	1.1	1.1	1.1	0.9	0.9	0.9	1.2
Yb	7.3	9.1	8.2	8.1	8.3	8.5	7.8	7.9	7.9	6.3	6.5	6.7	8.3
Lu	0.8	1.1	1	1	1	1	1	1	1	0.8	0.8	0.8	1.1

Table 5 Whole-rock Sm-Nd isotopic data for the Keimoes Suite granitoids and Koras Group volcanic rocks, eastern NMP

Sample	Rock type	Sm (ppm)	Nd (ppm)	Sm/Nd	$(^{143}Nd/^{144}Nd)_0$	2SE	$^{147}Sm/^{144}Nd$	$(^{143}Nd/^{144}Nd)_t$	$CHUR_{(t)}$	$\varepsilon_{Nd}(t)$	$\varepsilon_{Nd}(0)$	Age (Ma)	T_{CHUR}	T_{DM}	References
Koras Group															
Lower succession															
K2	Boom River basaltic andesite	4.7	21.8	0.216	0.512 113	14	0.130 414	0.511 146	0.511 179	-0.65	-10.24	1 130	1.206	1.894	Bailie et al. (2012)
K6	Boom River basaltic andesite	5.5	26.0	0.212	0.512 082		0.127 960	0.511 133	0.511 179	-0.90	-10.85	1 130	1.232	1.895	Bailie et al. (2012)
K11	Boom River basaltic andesite	6.0	28.2	0.213	0.512 090	11	0.128 702	0.511 135	0.511 179	-0.85	-10.69	1 130	1.227	1.897	Bailie et al. (2012)
K11B	Boom River basaltic andesite	6.0	28.2	0.213	0.512 048	30	0.128 702	0.511 093	0.511 179	-1.67	-11.51	1 130	1.321	1.972	This study
K14	Boom River basaltic andesite	5.0	23.3	0.215	0.511 981	12	0.129 807	0.511 018	0.511 179	-3.15	-12.82	1 130	1.494	2.118	Bailie et al. (2012)
W28	Boom River basaltic andesite	5.1	23.9	0.213	0.512 001	13	0.129 079	0.511 044	0.511 179	-2.65	-12.43	1 130	1.434	2.065	Bailie et al. (2012)
W29	Boom River basaltic andesite	5.1	23.7	0.215	0.512 032	12	0.130 168	0.511 066	0.511 179	-2.20	-11.82	1 130	1.386	2.035	Bailie et al. (2012)
K8	Swartkopsleegte rhyolite	16	86	0.186	0.512 301	28	0.112 540	0.511 466	0.511 179	5.62	-6.57	1 130	0.611	1.279	This study
K8B	Swartkopsleegte rhyolite	16.0	86.0	0.186	0.512 301		0.112 540	0.511 466	0.511 179	5.62	-6.57	1 130	0.611	1.279	This study
K20	Swartkopsleegte rhyolite	14.2	73.4	0.193	0.512 085		0.117 024	0.511 217	0.511 179	0.74	-10.79	1 130	1.058	1.677	Bailie et al. (2012)
Upper succession															
K12	Leeuwdraai rhyolitic porphyry	13.5	76.8	0.176	0.511 849	9	0.106 330	0.511 081	0.511 218	-2.67	-15.39	1 100	1.329	1.843	Bailie et al. (2012)
K12B	Leeuwdraai rhyolitic porphyry	14.8	87.4	0.169	0.511 828	22	0.102 432	0.511 088	0.511 218	-2.53	-15.80	1 100	1.308	1.808	This study
K13	Leeuwdraai rhyolitic porphyry	14.1	80.4	0.175	0.511 766	11	0.106 083	0.511 000	0.511 218	-4.26	-17.01	1 100	1.464	1.956	Bailie et al. (2012)
K21	Leeuwdraai rhyolitic porphyry	13.3	75.7	0.176	0.511 812	11	0.106 277	0.511 045	0.511 218	-3.39	-16.11	1 100	1.390	1.894	Bailie et al. (2012)
K22	Leeuwdraai rhyolitic porphyry	12.9	73	0.177	0.511 812	10	0.106 893	0.511 040	0.511 218	-3.47	-16.11	1 100	1.400	1.905	Bailie et al. (2012)
K23	Leeuwdraai rhyolitic porphyry	13.1	75.3	0.174	0.511 410	13	0.105 235	0.510 650	0.511 218	-11.10	-23.95	1 100	2.039	2.436	Bailie et al. (2012)
K23B	Leeuwdraai rhyolitic porphyry	14.2	86.4	0.164	0.511 795	19	0.099 416	0.511 077	0.511 218	-2.75	-16.44	1 100	1.319	1.804	This study
K31	Rouxville basaltic andesite	5.3	24.5	0.216	0.511 973		0.130 856	0.511 028	0.511 218	-3.71	-12.97	1 100	1.537	2.160	Bailie et al. (2012)
K37	Welgevind rhyolitic porphyry	17	103.3	0.165	0.511 824	7	0.099 548	0.511 105	0.511 218	-2.20	-15.88	1 100	1.276	1.767	Bailie et al. (2012)
K37B	Welgevind rhyolitic porphyry	18.5	118.2	0.157	0.511 866	21	0.094 676	0.511 182	0.511 218	-0.69	-15.06	1 100	1.153	1.642	This study
Keimoes Suite															
Mkb 6	Keboes granite	4.3	21.1	0.205	0.511 977	14	0.124 222	0.511 072	0.511 205	-2.60	-12.89	1 110	1.388	1.994	Bailie et al. (2017)
Mka 1	Kanoneiland granite	12.7	62.9	0.202	0.511 968	4.8	0.122 018	0.511 083	0.511 211	-2.52	-13.08	1 105	1.366	1.962	Bailie et al. (2017)
Mka 6	Kanoneiland granite	18.0	95.2	0.189	0.512 076	10	0.114 616	0.511 245	0.511 211	0.65	-10.96	1 105	1.043	1.650	Bailie et al. (2017)
Kan1	Kanoneiland granite	1.7	12.1	0.140	0.511 970		0.084 986	0.511 354	0.511 211	2.78	-13.03	1 105	0.912	1.396	This study
Gems	Gemsbokbult granite	14.0	77.9	0.180	0.511 984		0.108 711	0.511 197	0.511 214	-0.33	-12.76	1 103	1.132	1.690	Bailie et al. (2011a)
Mkle 1	Kleinbegin granite	9.8	46.4	0.210	0.511 698	7	0.127 310	0.510 778	0.511 217	-8.58	-18.34	1 101	2.058	2.552	Bailie et al. (2017)
Klein	Kleinbegin granite	13.7	88.7	0.154	0.511 643		0.093 429	0.510 968	0.511 217	-4.87	-19.41	1 101	1.466	1.906	Bailie et al. (2011a)

Table 5 Continued

Sample	Rock type	Sm (ppm)	Nd (ppm)	Sm/Nd	$(^{143}Nd/^{144}Nd)_0$	2SE	$^{147}Sm/^{144}Nd$	$(^{143}Nd/^{144}Nd)_t$	$CHUR_{(t)}$	$\varepsilon_{Nd}(t)$	$\varepsilon_{Nd}(0)$	Age (Ma)	T_{CHUR}	T_{DM}	References
Koras Group															
Upper succession															
Keimoes Suite															
Kle1	Kleinbegin granite	7.4	37.4	0.198	0.511 700		0.119 686	0.510 835	0.511 217	-7.46	-18.30	1 101	1.851	2.343	Bailie et al. (2017)
Mks 1	Klip Koppies granite	14.2	71.4	0.198	0.511 945	7	0.120 031	0.511 082	0.511 223	-2.77	-13.52	1 096	1.376	1.957	Bailie et al. (2017)
Klip K	Klip Koppies granite	14.6	74.6	0.196	0.512 022		0.118 385	0.511 170	0.511 223	-1.03	-12.02	1 096	1.198	1.801	Bailie et al. (2011a)
Klip	Klip Koppies granite	9.7	53.1	0.183	0.511 950		0.110 500	0.511 155	0.511 223	-1.33	-13.42	1 096	1.216	1.769	Bailie et al. (2017)
Mkl3	Klipkraal granite	108.6	576.8	0.188	0.511 970		0.113 891	0.511 140	0.511 205	-1.26	-13.03	1 110	1.228	1.799	Bailie et al. (2017)
MkI 4	Klipkraal granite	23.2	118.9	0.195	0.511 971	10	0.118 034	0.511 111	0.511 205	-1.84	-13.01	1 110	1.291	1.875	Bailie et al. (2017)
MkI 5	Klipkraal granite	23.6	129.5	0.182	0.511 923	8	0.110 069	0.511 121	0.511 205	-1.64	-13.94	1 110	1.256	1.801	Bailie et al. (2017)
Klp	Klipkraal granite	20.8	108.6	0.192	0.511 920		0.115 856	0.511 076	0.511 205	-2.52	-14.01	1 110	1.352	1.912	Bailie et al. (2017)
Strauss	Straussburg granite	11.6	58.0	0.200	0.511 970		0.120 980	0.511 105	0.511 232	-2.48	-13.03	1 089	1.343	1.936	Pettersson et al. (2007)
Str1	Straussburg granite	15.4	98.1	0.157	0.511 760		0.094 959	0.511 081	0.511 232	-2.95	-17.13	1 089	1.314	1.781	Bailie et al. (2017)
Mf 1	Friersdale charnockite	15.6	82.4	0.189	0.512 033	8.4	0.114 288	0.511 224	0.511 246	-0.43	-11.81	1 078	1.119	1.710	Bailie et al. (2017)
Mf 4	Friersdale charnockite	15.5	81.0	0.191	0.512 010	8.5	0.115 596	0.511 193	0.511 246	-1.05	-12.24	1 078	1.179	1.768	Bailie et al. (2017)
Mf 6	Friersdale charnockite	14.5	79.8	0.181	0.512 011	9.5	0.109 627	0.511 236	0.511 246	-0.21	-12.23	1 078	1.097	1.666	Bailie et al. (2017)
S188	Friersdale charnockite	14.2	79.4	0.179	0.512 030		0.108 181	0.511 265	0.511 246	0.36	-11.86	1 078	1.047	1.616	Bailie et al. (2017)
S815	Friersdale charnockite	14.4	78.8	0.183	0.512 010		0.110 540	0.511 228	0.511 246	-0.36	-12.25	1 078	1.110	1.682	Bailie et al. (2017)
S367	Friersdale charnockite	14.3	76.6	0.187	0.512 010		0.112 925	0.511 211	0.511 246	-0.69	-12.25	1 078	1.142	1.722	Bailie et al. (2017)
Friers 1	Friersdale charnockite	14.9	78.7	0.189	0.512 000		0.114 524	0.511 190	0.511 246	-1.11	-12.45	1 078	1.183	1.765	Pettersson et al. (2007)
Friers 2	Friersdale charnockite	14.7	77.4	0.190	0.511 980		0.114 884	0.511 167	0.511 246	-1.55	-12.84	1 078	1.225	1.802	Pettersson et al. (2007)

$(^{143}Nd/^{144})_{DM,0}$, the present day value of the depleted mantle (DM=0.513 15; $(^{147}Sm/^{144}Nd)_{DM,0}$, present day value of DM=0.213 6; $\varepsilon_{Nd}(t)$ calculated using $(^{143}Nd/^{144}Nd)_{CHUR}$ today=0.512 638 with $^{146}Nd/^{144}Nd$=0.712 90, $\varepsilon_{Nd}(0)$=$((^{143}Nd/^{144}Nd_{(0)}/0.512\ 638)-1)\times 10\ 000$; $\varepsilon_{Nd}(t)$=$((^{143}Nd/^{144}Nd_{(sample,t)}/^{143}Nd/^{144}Nd_{(CHUR,t)})-1)\times 10\ 000$; t in all equations is the time of emplacement of the granite/volcanics; $T_{DM}=1/(\lambda)\times\ln(1+(^{143}Nd/^{144}Nd_{(sample,0)}-{}^{143}Nd/^{144}Nd_{(DM,0)}/(^{147}Sm/^{144}Nd_{(sample,0)}-{}^{147}Sm/^{144}Nd_{(DM,0)})\times 10^{-9}$ (after DePaolo, 1981). $T_{CHUR}=1/(\lambda)\times\ln(1+(^{143}Nd/^{144}Nd_{(sample,0)}-{}^{143}Nd/^{144}Nd_{(CHUR,0)}/(^{147}Sm/^{144}Nd_{(sample,0)}-{}^{147}Sm/^{144}Nd_{(CHUR,0)})\times 10^{-9}$ (after DePaolo, 1981); $(^{147}Sm/^{144}Nd)_{CHUR}$ today=0.196 7; ages for the Koras Group lower succession are from Mothibi (2016); for the upper succession from Pettersson et al. (2007) and Bailie et al. (2012); ages for the various granites of the Keimoes Suite are from Bailie et al. (2017, 2011a) and Cornell et al. (2012).

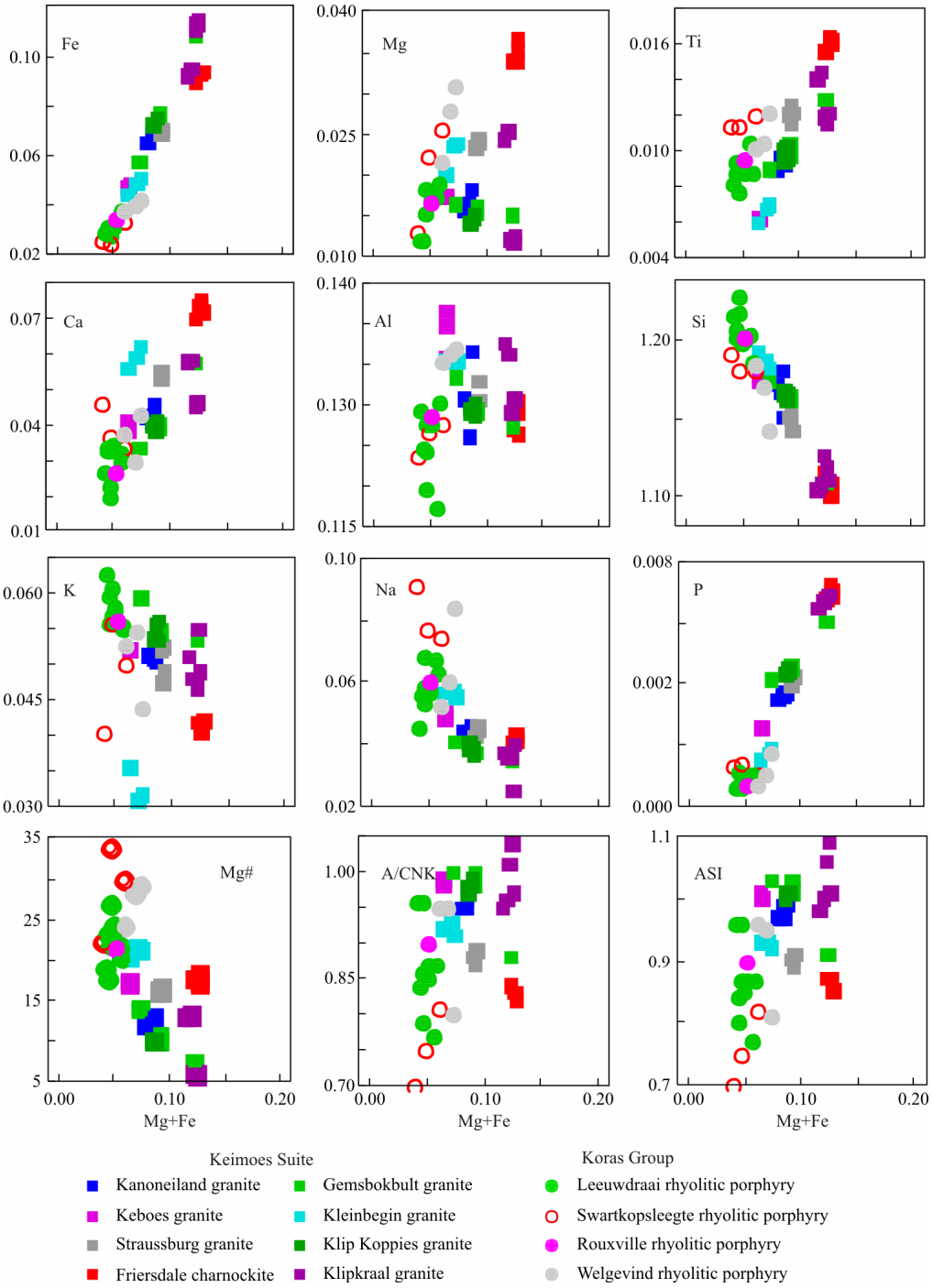

Figure 5. Maficity plots for major and minor elements of the Keimoes Suite granitoids and Koras Group rhyolitic porphyries.

vary from 0.652 82 to strongly radiogenic values of 0.771 30.

The lower succession basaltic andesites (Boom River Formation) have $^{143}Nd/^{144}Nd$ ratios (for the time of volcanism) and $\varepsilon_{Nd}(t)$ values which vary from 0.511 02–0.511 15, and -0.65 to -3.15, respectively. These are higher than those of a basaltic andesite sample of the upper succession (0.511 03 and -3.71, a sample of the Rouxville Formation). Likewise, the lower succession rhyolites have higher initial $^{143}Nd/^{144}Nd$ ratios (0.511 22–0.511 47) and $\varepsilon_{Nd}(t)$ values (0.74 to 5.62) than those of the upper succession (0.510 65–0.511 18, and -0.69 to -4.26, respectively, as well as a strongly negative value of -11.10: Table 6). The lower succession has a much younger model age range (T_{DM}: 1.28–2.12 Ga) compared to the upper succession (1.64–2.44 Ga). Such $\varepsilon_{Nd}(t)$ values suggest derivation from weakly depleted to mildly enriched sources and a probable mixture between juvenile Mesoproterozoic and older Paleoproterozoic sources. The lower succession is characterized by a greater depleted component than the upper succession, with the latter characterized by a greater crustal signature. There are only a few Rb-Sr isotopic data available, with initial $^{87}Sr/^{86}Sr$ ratios varying from 0.709 71 to 0.716 96. The upper succession has lower initial Sr ratios, in general, than the lower succession (Table 6).

Table 6 Whole-rock Rb-Sr isotopic data for the Keimoes Suite granitoids and Koras Group volcanic rocks, eastern NMP

Sample	Rock type	Rb (ppm)	Sr (ppm)	Rb/Sr	$(^{87}Sr/^{86}Sr)_0$	2SE	$^{87}Rb/^{86}Sr$	$(^{87}Sr/^{86}Sr)_t$	BSE(t)	$\varepsilon_{Sr}(t)$	Age (Ma)	References
Koras Group												
Lower succession												
K11B	Boom River basaltic andesite	71	307	0.23	0.724 609	12	0.612 581	0.714 700	0.703 325	161.7	1 130	This study
K8B	Swartkopsleegte rhyolite	198	186	1.06	0.758 735	18	2.827 621	0.712 997	0.703 325	137.5	1 130	This study
Upper succession												
K12B	Leeuwdraai rhyolitic porphyry	201	180	1.12	0.763 652	16	2.966 146	0.716 957	0.703 362	193.3	1 100	This study
K23B	Leeuwdraai rhyolitic porphyry	219	170	1.29	0.765 667	20	3.421 875	0.711 798	0.703 362	119.9	1 100	This study
K37B	Welgevind rhyolitic porphyry	190	232	0.82	0.743 957	16	2.175 377	0.709 711	0.703 362	90.3	1 100	This study
Keimoes Suite												
Mkb 6	Keboes granite	186	294	0.63	0.797 790	13	1.675 313	0.771 175	0.703 350	964.3	1 110	Bailie et al. (2017)
Mka 1	Kanoneiland granite	246	160	1.54	0.717 529	12	4.091 831	0.652 818	0.703 356	-718.5	1 105	Bailie et al. (2017)
Mka 6	Kanoneiland granite	233	143	1.63	0.791 095	14	4.333 226	0.722 566	0.703 356	273.1	1 105	Bailie et al. (2017)
kan1	Kanoneiland granite	130	533	0.24	0.717 529	12	0.645 751	0.707 317	0.703 356	56.3	1 105	Bailie et al. (2011)
Mkle 1	Kleinbegin granite	107	154	0.70	0.763 797	14	1.851 874	0.734 617	0.703 361	444.4	1 101	Bailie et al. (2017)
kle1	Kleinbegin granite	221	179	1.23	0.763 797	14	3.279 504	0.712 122	0.703 361	124.6	1 101	Bailie et al. (2017)
Klip	Klip Koppies granite	209	149	1.40	0.723 870		3.725 881	0.665 430	0.703 367	-539.4	1 096	Bailie et al. (2017)
Mkl3	Klipkraal granite	1 101	826	1.33	0.772 350		3.540 595	0.716 101	0.703 350	181.3	1 110	Bailie et al. (2017)
MkI 4	Klipkraal granite	204	147	1.39	0.772 353	14	3.694 668	0.713 656	0.703 350	146.5	1 110	Bailie et al. (2017)
MkI 5	Klipkraal granite	200	165	1.21	0.764 825	12	3.207 373	0.713 870	0.703 350	149.6	1 110	Bailie et al. (2017)
Klp	Klipkraal granite	175	161	1.09	0.764 825	12	2.886 942	0.718 960	0.703 350	221.9	1 110	Bailie et al. (2011)
Str1	Straussburg granite	158	228	0.69	0.746 117	11	1.839 839	0.717 445	0.703 375	200.0	1 089	Bailie et al. (2017)
Mf 1	Friersdale charnockite	157	279	0.56	0.736 655	14	1.488 460	0.713 695	0.703 389	146.5	1 078	Bailie et al. (2017)
Mf 4	Friersdale charnockite	161	277	0.58	0.734 338	15	1.546 078	0.710 489	0.703 389	100.9	1 078	Bailie et al. (2017)
Mf 6	Friersdale charnockite	159	264	0.60	0.734 072	15	1.601 357	0.709 370	0.703 389	85.0	1 078	Bailie et al. (2017)
S188	Friersdale charnockite	165	262	0.63	0.736 655	14	1.669 527	0.710 902	0.703 389	106.8	1 078	Bailie et al. (2011)
S815	Friersdale charnockite	165	277	0.60	0.734 338	15	1.580 713	0.709 954	0.703 389	93.3	1 078	Bailie et al. (2011)
S367	Friersdale charnockite	160	271	0.59	0.734 072	15	1.569 246	0.709 866	0.703 389	92.1	1 078	Bailie et al. (2011)

BA. Basaltic andesite; RP. rhyolitic porphyry.

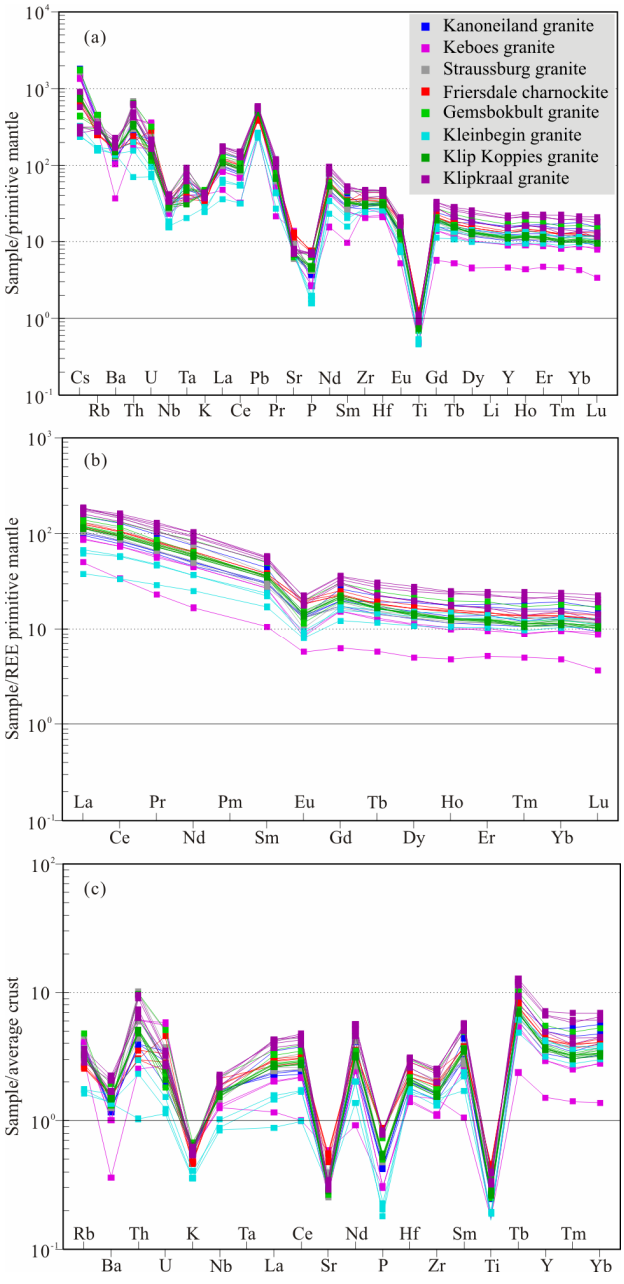

Figure 6. (a) Multi-element trace element plot (spider diagram) for the Keimoes Suite (normalised to the primitive mantle values of Sun and McDonough, 1989). (b) REE plot for the Keimoes Suite granites normalised to the primitive mantle values of McDonough and Sun (1995). (c) Multi-element trace element plot (spider diagram) for the Keimoes Suite normalised to the average crustal values of Weaver and Tarney (1984).

5 DISCUSSION

5.1 Sources

5.1.1 Keimoes Suite

The Keimoes Suite, despite being stratigraphically grouped as a suite, constitutes a number of plutons which, despite being temporally similar (~1.11–1.08 Ga) and spatially constrained to within one broadly defined region (Fig. 2), are genetically unrelated. They were derived from different sources and likely underwent different petrogenetic processes to give rise to the compositional variations within each pluton. They, therefore, do not form one coherent unit linked by a certain petrogenetic process.

The Keimoes Suite granitoids show a variable degree of derivation from basaltic- or amphibolitic-type sources (Figs. 10f, 11a–11c). These mafic components, in general, appear to comprise more than 50% of the source for the parental melts. Relatively mafic sources for the granites are also evident in their higher compatible element (Cr, Co, Ni, Cu and Sc) concentrations. Certain granites, such as the Friersdale charnockite and Klipkraal granite, were derived from predominantly mafic sources with some potential mantle input. There is, however, a substantial sedimentary component in the sources to some granites. The compositions of the Kanoneiland granite samples, for example, overlap those of calculated psammite-derived melts (Fig. 11b). In general, the Keimoes Suite granitoids have $\varepsilon_{Nd}(t)$ values around zero (-2.95 to 2.83), Meso- to Paleoproterozoic model ages (T_{DM}: 1.38–1.99 Ga) and relatively high initial Sr isotope ratios (0.717–0.798), suggesting derivation from relatively depleted sources with a variable enriched and/or crustal component. This is supported by enrichments in Pb, Th, U, and the LREE relative to the HREE, and the LILE relative to the HFSE, with depletions in Ba, Nb, Ta, Sr, Eu, Ti, Al_2O_3, V and Sc (Fig. 6; Bailie et al., 2017). The I-type characteristics of the granitoids, with biotite±hornblende±orthopyroxene as the main mafic minerals, their granodioritic compositions, and arc-like affinities (negative Nb-Ta, Ti and P anomalies), suggests derivation from mainly igneous sources, with a minor sedimentary component giving rise to dry parental magmas. The Keimoes Suite granitoids show an increasing maficity, metaluminous character, and general decreasing degree of fractionation with decreasing age, becoming more granodioritic concomitant with an increase in mafic minerals and decrease in K-feldspar content (Bailie et al., 2017). In addition, they become more aluminous and less alkalic with decreasing age. This suggests a greater depleted source component in the parental magmas with time.

The high Fe/Mg ratios (0.82–3.84, avg. 1.66), and high HFSE, LILE and REE contents of the granitoids, are, however, also suggestive of fractionated A_2-types (Eby, 1992) (Figs. 4g–4h, 13c). The granitoids were derived from partial melting of mid- to lower-crustal sources, such as amphibolites, and supracrustal material, in the form of meta-greywackes and mafic pelites, In terms of processes that can give rise to A-type granites, the partial melting of pre-existing crustal rocks, and a combination of both fractionation of mantle-derived basaltic magmas and crustal anatexis of granodioritic or tonalitic sources are likely to be the most relevant.

The Keimoes Suite granites were derived by dehydration melting at pressures varying from 6 to >10 kbar (Fig. 10g), indicating derivation from the mid- to lower crust. The Kleinbegin granite was likely derived from shallower melting (closer to 6 kbar), whereas the others were derived from deeper levels (predominantly 10 kbar and greater). The Klipkraal granite and Friersdale charnockite were likely derived from deeper depths, with a possible mantle component present.

The Klipkraal granite and the Friersdale charnockite are the most mafic members of the Keimoes Suite. The charnockitic nature of the Friersdale charnockite may be due to either partial melting of dehydrated lower crust that had suffered prior melt extraction (cf. Geringer et al., 1987 for enclaves in the

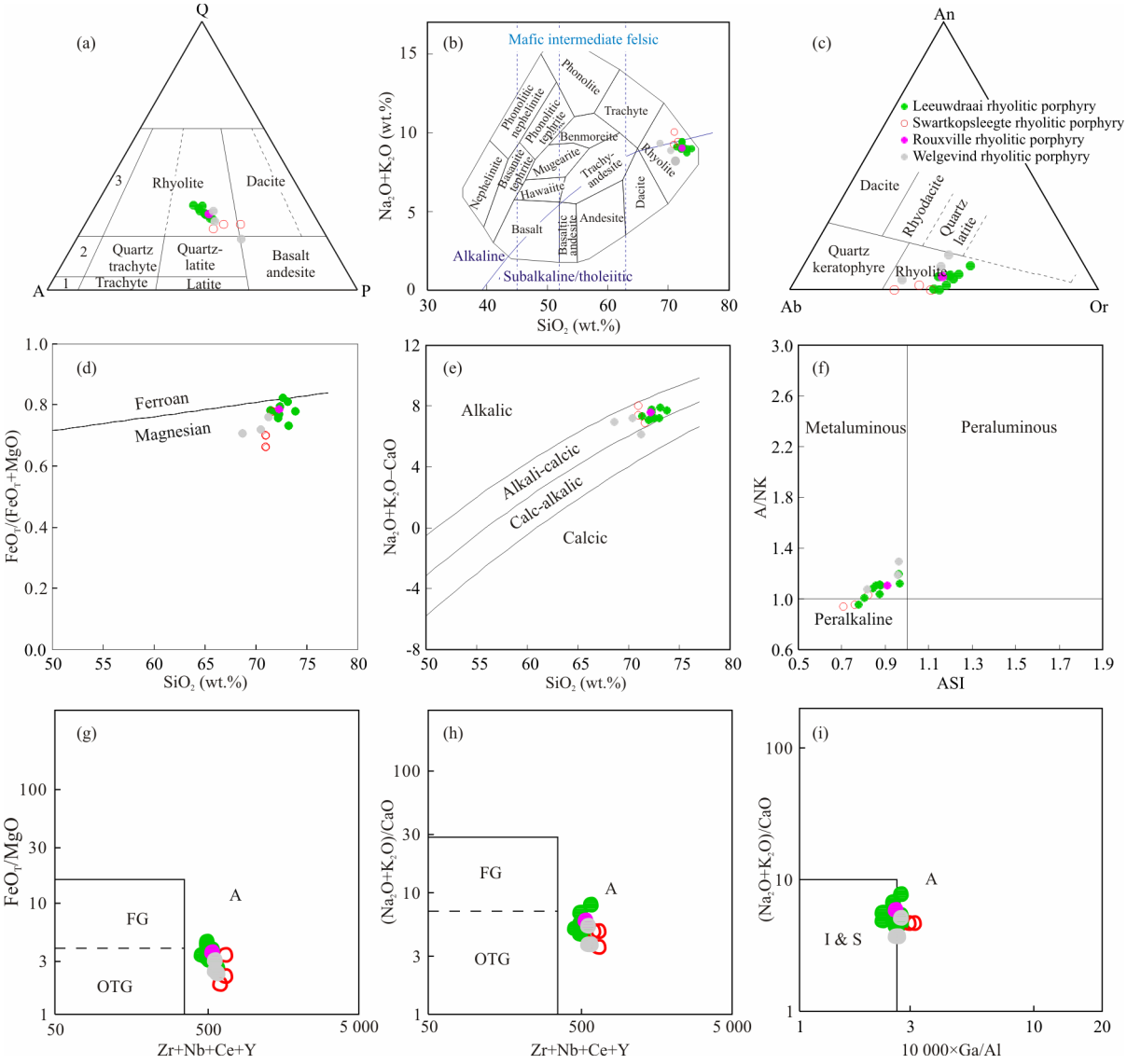

Figure 7. Classification plots for the Koras Group rhyolitic porphyries. (a) The QAP plot of Le Maitre et al. (1989); (b) the total alkalis vs. silica (TAS) plot of Cox et al. (1979); 1. alkali-feldspar trachyte; 2. q-alk-fsp trachyte; 3. alk-fsp rhyolite; (c) the An-Ab-Or ternary volcanic plot (after O'Connor, 1965); (d) $FeO_T/(FeO_T+MgO)$ vs. SiO_2 plot (after Frost et al., 2001); (e) the Na_2O+K_2O–CaO vs. SiO_2 plot (after Frost et al., 2001); (f) the molar $Al_2O_3/(Na_2O+K_2O)$ (A/NK) vs. aluminium saturation index (ASI) plot of Frost et al. (2001); (g) the FeO_T/MgO vs. Zr+Nb+Ce+Y plot of Whalen et al. (1987); (h) the $(K_2O+Na_2O)/CaO$ vs. Zr+Nb+Ce+Y plot; (i) the $(K_2O+Na_2O)/CaO$ vs. 10 000×Ga/Al plot of Whalen et al. (1987).

Straussburg granite compositionally similar to the Friersdale charnockite), or from a CO_2-enriched crust with some mantle input (Fig. 10d), although the tectonic setting of the Keimoes Suite, related to transtensional rift zones (Bailie et al., 2017), likely favours the melting of continental crust above an upwelling mafic magma, represented by the mafic magmas of the Koras Group. By contrast, the Kleinbegin and Keboes granites were derived by partial melting of crustal material (Fig. 10d), as also seen in their strongly negative $\varepsilon_{Nd}(t)$ values (Fig. 9).

Sm-Nd isotope characteristics (low $\varepsilon_{Nd}(t)$, variable model ages, and arc-related characteristics suggest the involvement of both juvenile Mesoproterozoic crust, such as the ~1.3–1.24 Ga Areachap arc (Pettersson et al., 2007), as well as the reworking of older ~1.80–2.2 Ga Paleoproterozoic crust (such as the 1.8–1.82 Ga Gladkop Suite, and the ~2.2 Ga Sperrgebiet and ~1.9 Ga Richtersveld arcs; Fig. 9b; Nke et al., 2020; Macey et al., 2018, 2017; Thomas et al., 2016). Mixing of different aged sources is likely (cf. the hybrid origin of Cornell et al., 2012), as seen in the spread of model ages and $\varepsilon_{Nd}(t)$ values (e.g., the Kanoneiland granite). Some granites (e.g., the Friersdale charnockite and Kanoneiland granite) have a larger juvenile source component, whereas others may have had potential Archean crustal source contributions (those with model ages ≥2.5 Ga). The reworking and contribution of these varying sources to the parental melts is evident by the presence of inherited zircons in some of the granitoids (Bailie et al., 2011a). The relatively low initial Sr ratios [$(^{87}Sr/^{86}Sr)_i$] for most of the granitoids (Fig. 9a) does, however, suggest that the parental magmas were largely derived from relatively unradiogenic sources. The lack of sufficient samples precludes evaluating the role of mixing in influencing compositional variation.

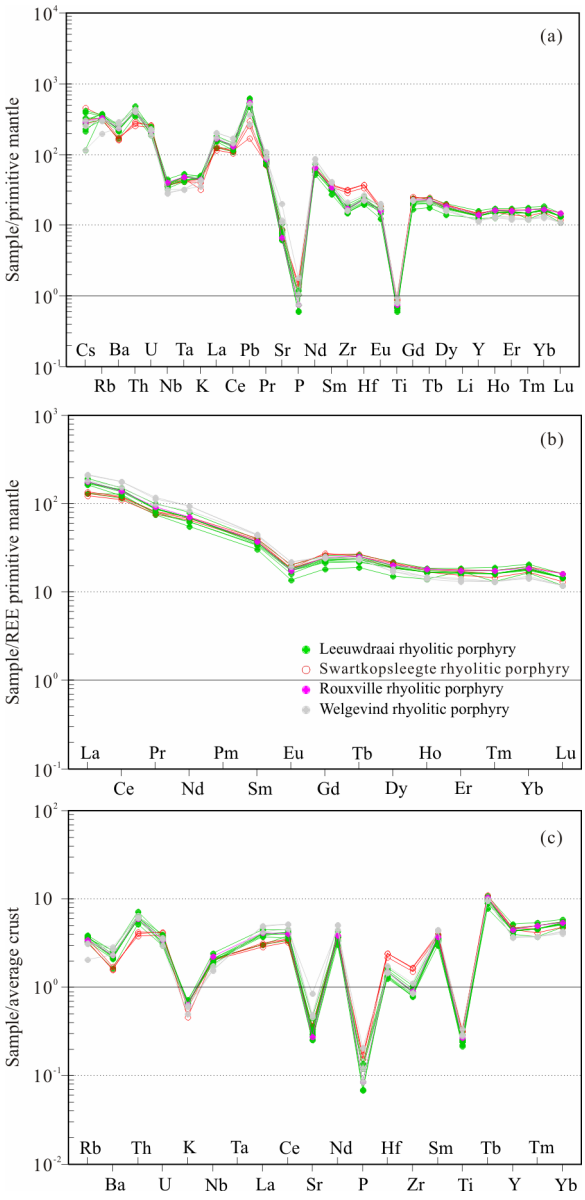

Figure 8. (a) Multi-element trace-element plot (spider diagram) for the rhyolitic porphyries of the Koras Group (normalised to the primitive mantle values of Sun and McDonough, 1989). (b) REE plot for the Koras Group rhyolitic porphyries normalised to the primitive mantle values of McDonough and Sun (1995). (c) Multi-element trace-element plot for the rhyolitic porphyries of the Koras Group normalised to the average crustal values of Weaver and Tarney (1984).

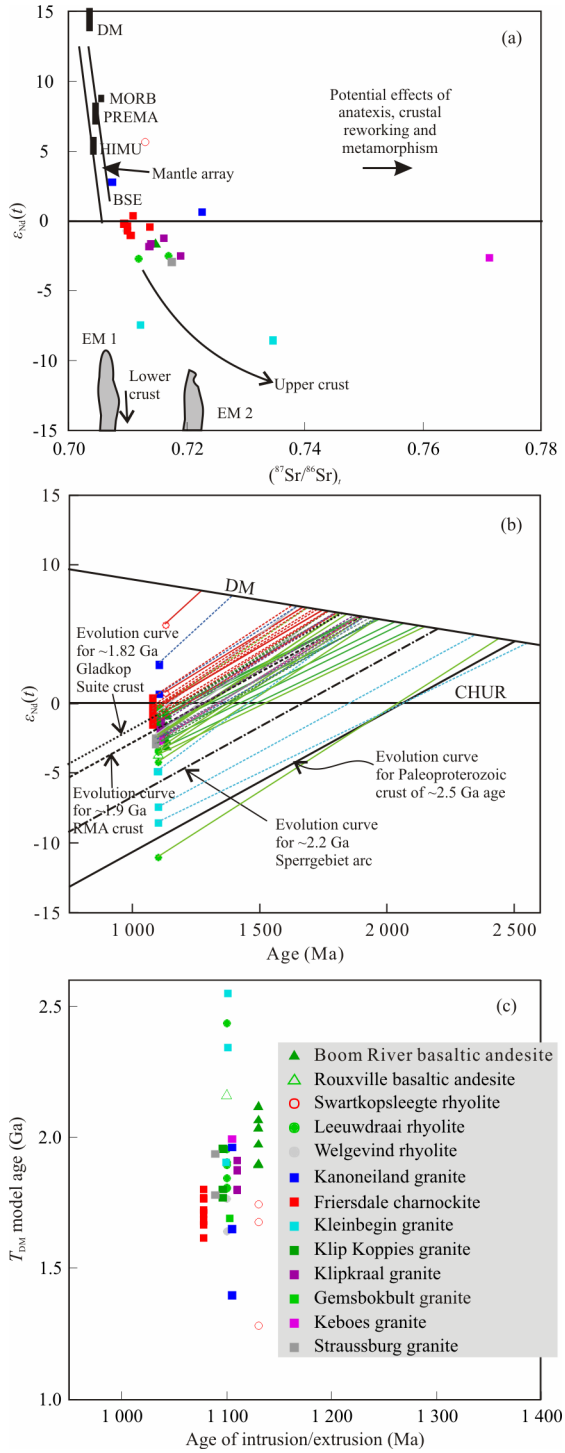

Figure 9. Sr-Nd isotopic plots for the Keimoes Suite granitoids and Koras Group volcanics. (a) $\varepsilon_{Nd}(t)$ vs. initial Sr ($Sr_i=(^{87}Sr/^{86}Sr)_i$, where i is the time of emplacement or volcanism). (b) $\varepsilon_{Nd}(t)$ vs. age. (c) Model age (T_{DM}) vs. age of extrusion or intrusion.

5.1.2 Koras Group

The Koras Group basaltic andesites were derived from the partial melting of lithospheric mantle wedge sources affected by fluid-related subduction metasomatism (Fig. 10e; Becker et al., 2000; McCulloch and Gamble, 1991). The basaltic andesites of the lower succession were derived from partial melting of spinel lherzolite within a variably enriched shallow mantle source (Fig. 10d; Fig. S6c). Subduction and mantle metasomatism related to the development of a continental to island arc had ceased some 50–80 million years prior to the time of Koras Group volcanism (e.g., Pettersson et al., 2007). The low incompatible element content of both successions indicates relatively high degrees of partial melting (Bailie et al., 2012). The geochemical and isotopic characteristics of the rhyolitic porphyries of both successions, including enrichment in the LILE relative to the HFSE, LREE/HREE enrichment, enrichment in compatible elements (Cu, Cr, Ni, V, Sc) and certain HFSE (Th, U, Pb), a negative Nb-Ta anomaly, and positive to mostly weakly negative $\varepsilon_{Nd}(t)$ values, suggest derivation from weakly depleted sources.

The lower succession is more mafic and has a greater depleted component to the parental magmas, whereas the upper succession is more felsic and fractionated and was derived from melts having a greater crustal component, as denoted by much lower $(Nb/Th)_{PM}$ and higher $(Th/Yb)_{PM}$ ratios (Bailie et al., 2012), becoming more felsic higher in the succession. The upper succession rhyolitic porphyries were likely derived by partial melting of Paleoproterozoic-aged crustal material (T_{DM}: 1.64–2.44 Ga) (Table 5). This melting was likely due to the heat caused by rifting and the influx of mantle-derived mafic melts (represented by the basaltic andesites), as opposed to being derived by fractional crystallisation of the latter. Lack of sufficient samples of basaltic andesites of the upper succession makes it difficult to assess any potential links between the two. The higher LREE/HREE, Th/Yb and Th/Ta, and lower Nb/Th, Nb/Y and Nb/Zr ratios of the rhyolites of the Northern Domain compared to those of the correlative Central Domain suggests a greater crustal contribution to the parental magmas of the former compared to the latter.

The lower succession rhyolites have trace element contents suggestive of derivation from mostly sedimentary-based sources (predominantly >80%) (Figs. 10f, 10g, 11a, 11b), with psammites or greywackes being the predominant source rock types. The lower succession rhyolites are variable in terms of $\varepsilon_{Nd}(t)$ values and model ages (Table 5), suggesting derivation from variable sources and potential mixing. With Paleo-

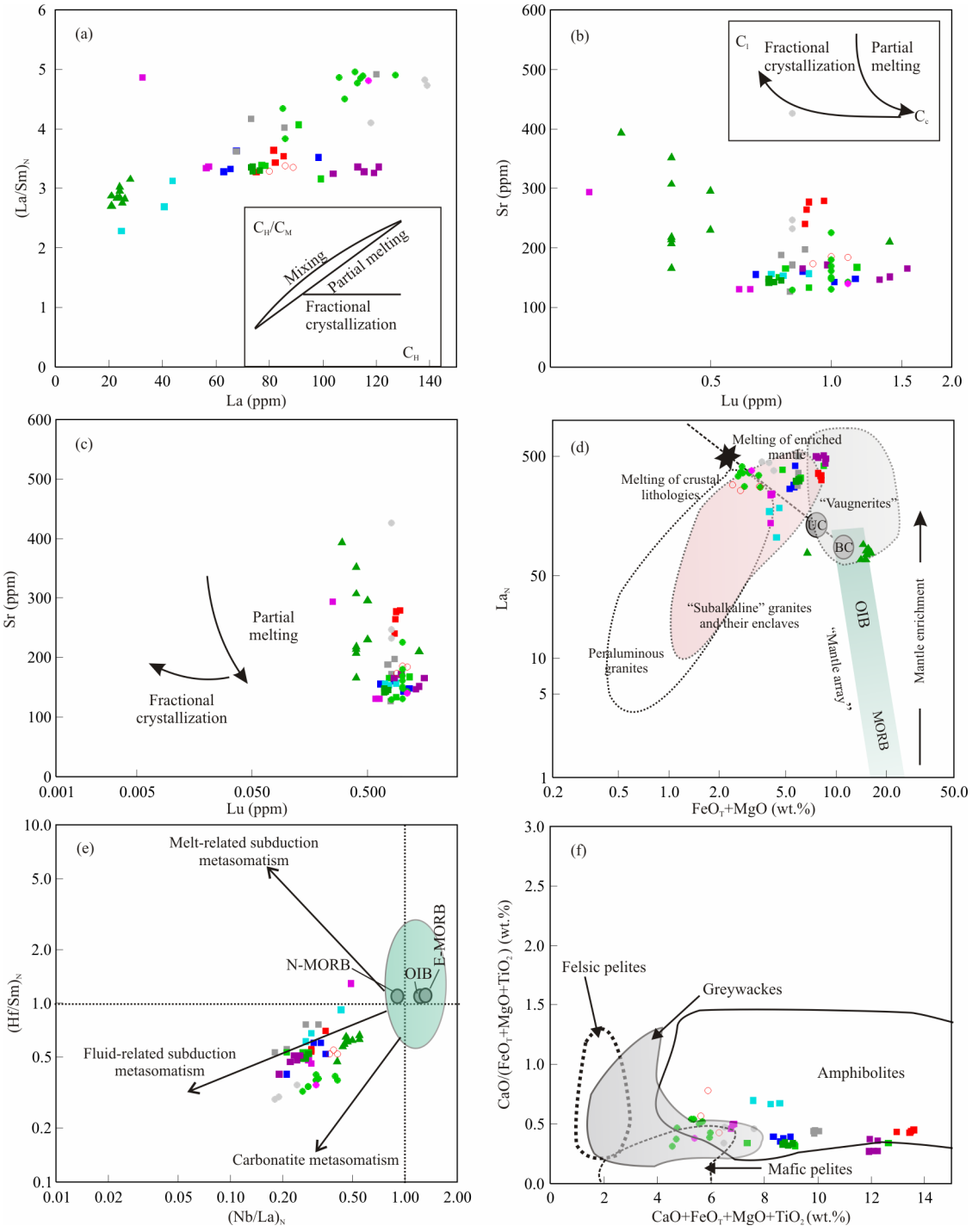

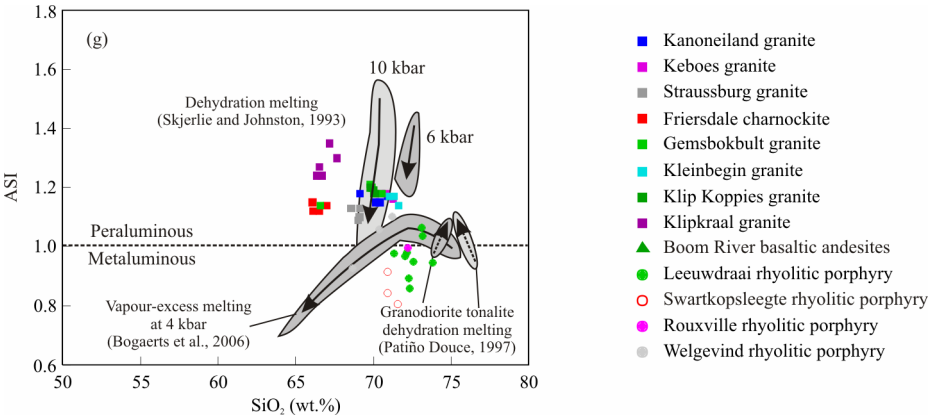

Figure 10. Petrogenetic diagrams of the Koras Group volcanics and Keimoes Suite granitoids. (a) $(La/Sm)_N$ vs. La diagram, where the N subscript represents chondrite normalization, showing the trajectories of partial melting, fractional crystallization, and magma mixing. The inset is a schematic C_H/C_M vs. C_H plot, where H and M are highly and moderately incompatible elements, respectively. (b) Sr versus Lu diagram showing trajectories of partial melting and fractional crystallization (after Peccerillo et al., 2003). Sr and Lu are incompatible and compatible elements, respectively (Rollinson, 1993). (c) Sr vs. Lu diagram, showing that the genesis of K-rich granitoids are controlled dominantly by partial melting (Rollinson, 1993), as also seen for the Keimoes Suite granitoids. (d) La_N vs. FeO_T+MgO diagram (after Laurent et al., 2014) with BC representing bulk crust, and UC, upper crust, OIB ocean island basalt, and MORB, mid-ocean ridge basalt. (e) $(Hf/Sm)_N$ vs. $(Nb/La)_N$ diagram (after La Fléche et al., 1998). The N subscript represents chondrite normalization; E-MORB is enriched MORB and N-MORB, normal MORB. (f) $CaO/(FeO_T+MgO+TiO_2)$ vs. $CaO+FeO_T+MgO+TiO_2$ diagram. The fields represent compositions of experimentally-derived partial melts from amphibolites, greywackes, and mafic and felsic pelites (after Patiño Douce, 1999). (g) ASI (aluminium saturation index; $Al/(Ca-1.67P+Na+K)$ versus SiO_2 diagram (after Frost and Frost, 2011).

proterozoic model ages (T_{DM}: 1.89–2.12 Ga) and low negative $\varepsilon_{Nd}(t)$ values (-0.65 to -3.15; Table 6), the basaltic andesites were derived from partial melting of weakly to moderately depleted sources. The Sr_I of the Koras Group volcanics are relatively low (less than 0.72) suggesting derivation from weakly radiogenic sources.

The Koras Group rhyolites also show characteristics of A_2-type magmas (Figs. 7g–7i). A_2-type magmatism occurs shortly (10 to 20 million years, or longer) after periods of compressional tectonics (Eby, 1992). In terms of trace elements for A_2-type felsic magmatism, both subcontinental lithosphere and crustal source signatures are present, but never OIB-like signatures (Eby, 1992). This suggests that there was no influence of any kind of plume at ~1 100 Ma in the eastern Namaqua Province, as has been argued (e.g., Cornell et al., 2012).

5.2 Petrogenesis

5.2.1 Keimoes Suite

The general geochemical characteristics of the Keimoes Suite granitoids are summarized in Table 7 which includes geochemical and potential source characteristics. The limited number of samples, particularly of the individual granites, makes petrogenetic interpretation difficult and warrants further and more detailed studies. Variable amounts of partial melting can bring about variations in the abundances of moderately compatible elements, such as the LREE and Sr, whereas more strongly compatible elements, such as the HREE, most notably Lu, are more strongly influenced by fractional crystallisation, being taken up, in particular, by garnet (notably the HREE) and by accessory phases such as apatite, zircon or monazite. Plots of Sr against Lu (Figs. 10b, 10c) give rise to curved paths for these elements during variable amounts of partial melting due to their moderately compatible versus more compatible behaviour, with Sr able to go into the melt. This may imply that a phase in the residua would retain Lu, Y and other REE and liberate Sr. This phase is likely to be garnet because plagioclase would have the opposite effect (Chiaradia, 2015). By contrast fractional crystallisation leads to flatter patterns due to the compatible nature of both elements.

In terms of differentiating between the effects of partial melting and fractional crystallisation on compositional variation in the granites, certain granites, such as the Friersdale charnockite and Gemsbokbult granite, show trends that suggest that variable degrees of partial melting have brought about some compositional variation (Figs. 10a, 10b). By contrast, the flat trends shown by some granites on these plots, such as the Klipkraal granite, most notably, and possibly the Kleinbegin granite, suggest that fractional crystallisation played a role in bringing about compositional variation. The variations seen in both spider diagram and REE plots between the granites (Fig. 6) suggest that source heterogeneities brought about the inherent compositional differences between the granites, as also seen in terms of differing maficity and isotopic characteristics.

The fractional crystallisation of plagioclase and K-feldspar has brought about some compositional variation for most of the granites, particularly with regard to the LILE (Ba, Rb, Sr) and the alkalis (Fig. 12), but mostly as a later superimposed effect on the primary source-related compositional variation. Plagioclase retention or removal from the parental magma by fractional crystallisation would explain the prominent negative Eu and Sr anomalies in the spider diagrams, given that garnet would retain Y and the HREE and release Sr during melting (Fig. 6).

The lack of a sufficient number of samples per pluton, as well as differing age relationships, precludes the assessment of whether peritectic assemblage entrainment (PAE) may have played a role in the Keimoes Suite granitoids. PAE is a process that has been invoked to explain the compositional variation seen in both S- and I-type granites which cannot be produced

Table 7 General geochemical properties for the Keimoes Suite granitoids and generalized petrogenesis and source characteristics

Granite	Overall composition	Maficity	Major- and minor-elements	Trace-elements	Sm-Nd isotopes T_{DM} (in Ga)	Potential petrogenesis and sources
Klipkraal	Granodiorite to monzogranite calc-alkalic, ferroan, weakly peraluminous	High (second highest)	High: Fe (highest), Ti, P, ASI (highest); Low: Si, Na, high K_2O/Na_2O; high Fe/Mg	High: La, Sm, Eu, Y, Yb, Nb, Zr, Hf, Th, Ba, Pb, Sc Low: Sr	Low -ve $\varepsilon_{Nd}(t)$, high initial Sr (> 0.714); T_{DM}: 1.89–1.91	Unfractionated, mafic source, sedimentary component; I-/A-type characteristics; deep melting; inheritance from ~1.27 Ga Areachap arc
Kleinbegin	Granodiorite, magnesian, calcic, metaluminous, rel. Kfs-rich	Low (among lowest)	High: Si (highest), Ca, Al, Na (highest); Low: alkalis, Ti (lowest), Fe, K (lowest), Mn, P (lowest), ASI, K_2O/Na_2O	High: Ni, Cu; Low: La, Sm, Eu, Yb, Nb, Zr, Hf, Th, Rb, Ba, Pb, U, Sc	v. -ve $\varepsilon_{Nd}(t)$, high initial Sr (>0.712); T_{DM}: 1.91–2.55	Fractionated; old, radiogenic crust (>2.0 Ga) derivation; significant mafic igneous component; I-type; various sources, mostly >2.3 Ga; relatively shallow melting
Keboes	Monzogranite, w. pealuminous, calc-alkalic, ferroan, Qtz-rich	Lowest	High: Si, Al (highest); Intermediate: K; Low: Ti, Fe, Ca, Mn, P, K_2O/Na_2O	High: Rb, U; Low: La, Sm, Eu, Y, Yb, Nb, Zr, Hf, Ba, Co, Sc, (Ni)	Low -ve $\varepsilon_{Nd}(t)$, high initial Sr (>0.771, n=1); T_{DM}: 1.99	Amongst most fractionated; crustal derivation, substantial radiogenic sedimentary source; inherited zircons; feldspathic (Kfs-rich)
Gemsbokbult	Monzogranite, calc-alkalic, ferroan, weakly peraluminous	Variable (intermediate-high)	High: K (highest), P; Low: Mg, Ca, Na high Fe/Mg	Mostly intermediate; Low: V, Co, Sr, U	$\varepsilon_{Nd}(t)$ -ve but close to 0; no Sr data; T_{DM}: 1.69	Relatively fractionated; mildly depleted source, sedimentary component; lack of sufficient data for interpretation
Kanoneiland	Monzogranite, calc-alkalic, ferroan, weakly per- to metaluminous	Intermediate	High: Si; Low: Mg, Ti, Ca, ASI low K_2O/Na_2O; high Fe/Mg	Mostly intermediate; High: Rb; Low: Ba, Sr, Co, Cu, (Ni)	+ve $\varepsilon_{Nd}(t)$; variable to high initial Sr; T_{DM}: 1.40–1.96	Relatively fractionated; depleted source; juvenile crustal derivation; substantial sedimentary source (psammite?); Bt-rich; I-type; mix from various sources
Klip Koppies	Monzogranite; ferroan; quartz-rich; calc-alkalic; weakly peraluminous	Intermediate	High: Si, ASI, Fe/Mg; Low: Mg, Ti, Ca, ASI	High: LREE relative to HREE (high $(La/Yb)_N$); high $(Eu/Eu^*)_N$ Low: V, Co, Cu, Sr, U	Low -ve $\varepsilon_{Nd}(t)$, relatively low initial Sr value; T_{DM}: 1.77–1.96	Crustal derivation with minor depleted source contribution; sedimentary component (psammitic); inheritance from Areachap Group arc
Straussburg	Granodiorite-monzogranite; calc-alkalic, ferroan, metaluminous	Intermediate	High: Mg, Ca; Low: Si, K, ASI (lowest)	High: V, Zr, Hf, Th, (Co), (Ni); Low: Y, Yb	Low -ve $\varepsilon_{Nd}(t)$, moderate initial Sr (0.717, n=1); T_{DM}: 1.78–1.94	Relatively unfractionated; mildly enriched source (mostly igneous-rich); Hbl-bearing; mix of various-aged sources
Friersdale charnockite	Granodioritic-monzogranitic; calcic-calc-alkalic; ferroan; most metaluminous of Keimoes Suite	Highest	High: Fe, Mg (highest), Ti (highest), Ca (highest), P (highest), Mn; Low: Si (lowest), Al, K	High: Sr, Eu, Zr, Hf, Sc, V, Co, Ni, Cu, Nb; Low: Rb, Th, Pb	Low +ve to low -ve $\varepsilon_{Nd}(t)$, low initial Sr (<0.714); T_{DM}: 1.62–1.80	Relatively unfractionated (least fractionated of Keimoes Suite); depleted to weakly enriched source; substantial juvenile component (largely mafic igneous source); plagioclase fractionation; mixture of various sources; I-type

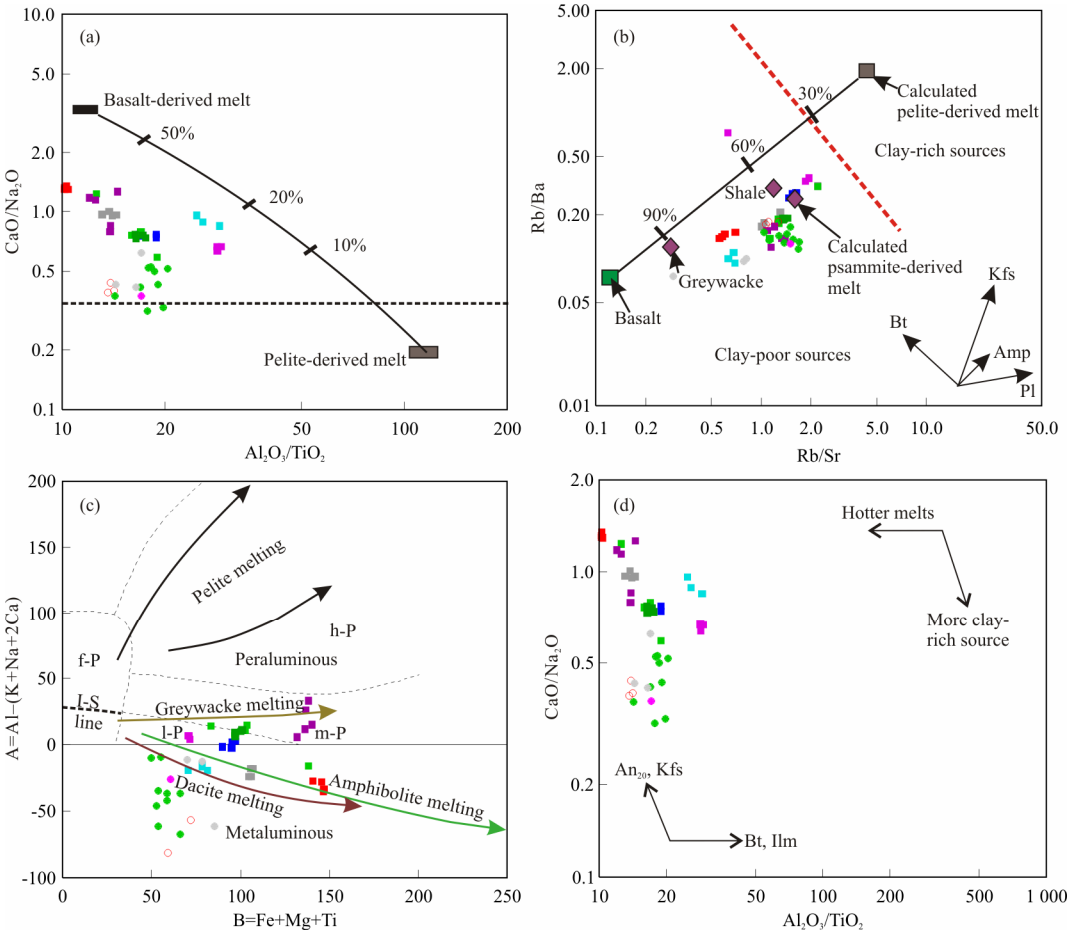

Figure 11. Test of source characteristics to the parental melts of the Koras Group volcanics and Keimoes Suite granitoids. (a) CaO/Na_2O vs. Al_2O_3/TiO_2. (b) Rb/Ba vs. Rb/Sr. The mixing curve between basalt- and pelite-derived melts is from Patiño Douce and Harris (1998) and Sylvester (1998). (c) A-B diagram (after Villaseca et al., 1998). The arrows represent the compositions of progressive melt fractions produced by experimental melting of different crustal rocks (Villaseca et al., 1998 and references therein). Highly, moderately, low and highly felsic peraluminous granitoids, are indicated by h-P, m-P, l-P and f-P respectively. (d) CaO/Na_2O vs. Al_2O_3/TiO_2 plot. Vectors for fractional crystallization of oligoclase (An_{20}), K-feldspar (Kfs), biotite (Bt) and ilmenite (Ilm), and for illustrating compositional variations with increasing melting temperature and clay components in the source are from Sylvester (1998) and references therein.

simply by fractional crystallisation or partial melting reactions (Clemens and Stevens, 2012; Clemens et al., 2011; Stevens et al., 2007). PAE refers to the process of entrainment of peritectic minerals or mineral assemblages produced during incongruent melting of the original source material. The peritectic assemblage produced and, potentially, entrained into the melt is dependent on the composition of the source material, among other factors. The PAE process can be assessed by correlations between maficity (molar Fe+Mg) and other major and minor elements (given in molar abundances).

Certain compositional variations within the Keimoes Suite granitoids (as shown by positive linear correlations on maficity plots for such elements as Fe, Mg, Ti, Ca, P and ASI for many of the granites, such as the Friersdale charnockite; Fig. 5), may be due to the entrainment of clinopyroxene+plagioclase (for Fe, Mg and Ca) and a Ti-bearing phase (such as ilmenite) for Ti. Such an assemblage would likely be produced by the incongruent melting of predominantly igneous biotite- ±hornblende-bearing sources (Clemens et al., 2011). The higher the maficity the greater the amount of entrained peritectic assemblage which is subsequently dissolved into the melt. The positive correlations of Fe, Mg and Ti against maficity are due to the entrainment and dissolution of the Fe-, Mg- and Ca-rich peritectic assemblage (dominated by clinopyroxene and plagioclase) into the melt. Dissolution of the pyroxenes and such Ti-bearing peritectic phases as ilmenite or titano-magnetite lead to a strong increase in Ti with increasing maficity. The entrainment of plagioclase influences the Ca content of the magma. Entrainment of such an assemblage can also produce a decrease in K with increasing maficity, as seen for some of the granites (Fig. 5) which would not be produced by the fractionation of Ti-bearing minerals (such as biotite and/or hornblende). Being incompatible, K concentrations would be high in pure melts, but its concentration is diluted by a greater amount of entrainment of K-poor peritectic phases and their dissolution into the magma. The positive correlation of P against maficity (Fig. 5) has been used to suggest the co-entrainment, and subsequent dissolution, of apatite, the major P-bearing mineral, into a granitic parental melt (Clemens et al., 2011). The poorly defined, slightly negative trends for Na, K and Rb against maficity (Fig. 5) suggest, however, that these reflect the fractionation of alkali feldspars (e.g., Villaros et al., 2009). These

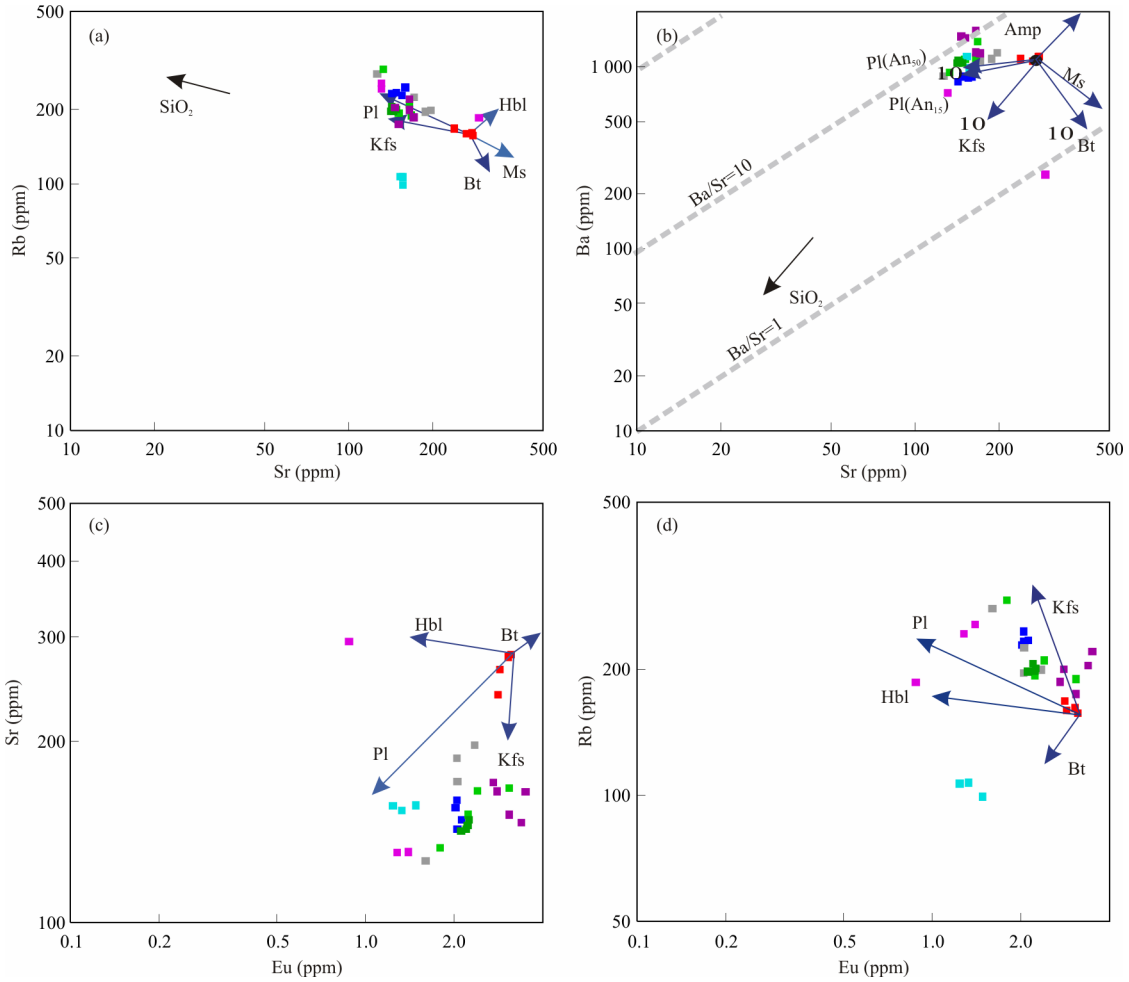

Figure 12. Binary plots testing the effects of fractional crystallisation of various minerals on the compositional variation within the Keimoes Suite granites. (a) Rb vs. Sr; (b) Ba vs. Sr; (c) Sr vs. Eu; (d) Rb vs. Eu.

elements act in an incompatible fashion and are taken up into the magma during melting, being concentrated in the first melts. Fractional crystallisation of the feldspars would give rise to negative trends with increasing maficity. More detailed studies, with a significantly larger number of samples per pluton, would be required to more rigorously assess the potential of PAE as a compositional driver in the granites.

The youngest granites (the Friersdale charnockite and Straussburg granite) have the highest maficity values and are also the most metaluminous (lowest A/CNK) (Figs. 4, 5). By contrast, the oldest members of the Keimoes Suite (e.g., the Keboes granite), which are largely leucocratic, and also weakly metaluminous and garnet-bearing, have the lowest maficity (Fig. 5). Peraluminous leucogranites with low maficities are considered to represent pure sedimentary crustal melts in high-grade regional metamorphic settings (e.g., Bial et al., 2015; Jung et al., 2012).

5.2.2 Koras Group

In terms of compositional variations caused by partial melting as opposed to fractional crystallisation (Figs. 10a–10c), the rhyolites of the upper succession, and basaltic andesites of the lower succession show trends on these plots suggesting that variable degrees of partial melting brought about some of their compositional variation. By contrast, the flat-lying trends of the lower succession rhyolites (Figs. 10a–10c) suggests that fractional crystallisation played a greater role in compositional variation than did variable amounts of partial melting.

The mafic and felsic lavas of both successions show regular differentiation trends related to progressive fractional crystallisation (Fig. 13), explaining the trend from the basaltic andesites to the rhyolitic porphyries of the lower succession, in particular (Bailie et al., 2012). K-feldspar and plagioclase fractionation (more evident on the Sr plots), with lesser amounts of biotite (±hornblende), such as in the Welgevind Formation, where Fe variation is a larger factor (Fig. 13), likely brought about the compositional variation seen. The rhyolites of the Swartkopsleegte Formation, of the lower succession, are controlled by Na and Ca (likely due to plagioclase), whereas those of the upper succession are controlled by Si and K (likely K-feldspar). A slight negative Zr trough in the multi-element plot (Fig. 8) possibly suggests zircon fractionation. The basaltic andesites were affected by crustal contamination (Bailie et al., 2012; Fig. S6a).

The rhyolites do not form distinctive trends on any maficity plots (Fig. 5), apart from relatively well-defined negative correlations of Si and K with maficity. This suggests that PAE probably did not play a significant role in determining the

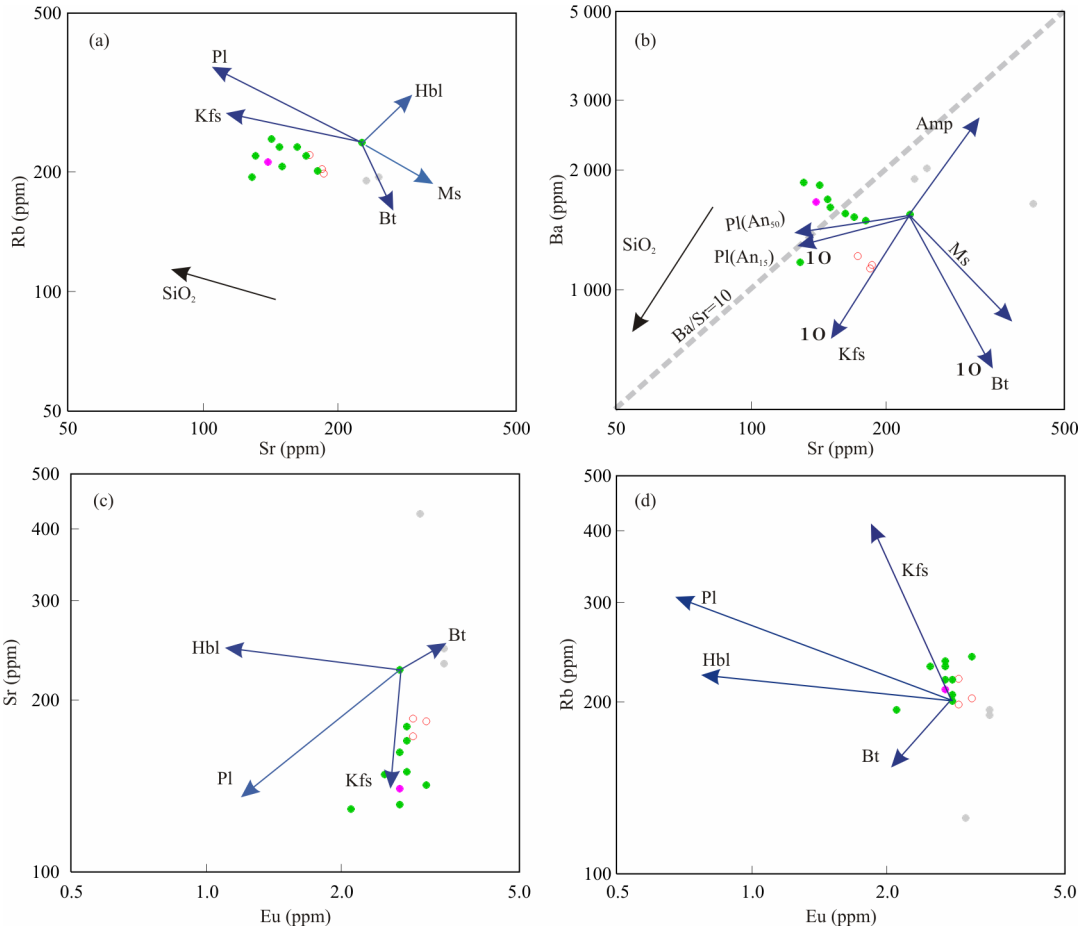

Figure 13. Binary plots testing the effects of fractional crystallisation of various minerals on the compositional variation within the Koras Group volcanic rocks. (a) Rb vs. Sr; (b) Ba vs. Sr; (c) Sr vs. Eu; (d) Rb vs. Eu.

compositional variation in the Koras Group, although, again, more samples and more detailed study is required.

5.3 Implications for the Post-Collisional Tectono-Magmatic Evolution of the Eastern Namaqua Metamorphic Province

The western margin of the Kaapvaal Craton developed as a passive margin. Initially sedimentation was fluvial in the form of braided rivers, but with rifting, a shallow open sea developed, on the margin of which shallow marine sediments were deposited (the bulk of the Keis Supergroup; Van Niekerk and Beukes, 2019).

At ~1.35 Ga subduction was initiated, leading to development of a volcanic arc, represented by the Areachap Group, on the western margin of the Kaapvaal Craton due to eastward-directed subduction (Bailie et al., 2010; Cornell and Pettersson, 2007; Pettersson et al., 2007; Geringer et al., 1986). The Areachap arc developed between ~1.3 and 1.25 Ga, having a greater continental signature toward the north and was more juvenile toward the south. Closure of the Areachap Sea commenced at ~1.22 Ga and likely continued until ~1.15–1.13 Ga giving rise to extensive eastward-directed thrusting (Van Niekerk and Beukes, 2019, and references therein). The sea which had developed due to extensional forces was closed leading to eastward-directed thrusting onto the western margin of the Kaapvaal Craton, and westward-directed thrusting onto the Bushmanland Subprovince along the Hartbees River thrust toward the west with the Areachap and Kakamas domains caught in between. Accretion of the Areachap arc onto the western margin of the Kaapvaal Craton likely led to widespread magmatism giving rise to the pre- to syn-tectonic granitic gneisses of the Areachap and Kakamas Domains (Bailie et al., 2017; Bial et al., 2015) and upper amphibolite facies M_2 metamorphism reaching its peak at ~1.16–1.15 Ga (Cornell and Pettersson, 2007; Pettersson et al., 2007).

The lateral escape of the Areachap and Kakamas domains was brought about by prolonged compression which resulted in a releasing bend in the eastern NMP (Sithole, 2013; van Bever Donker, 1991). Potential slab roll-back led to the opening of a rift along the former back-arc region of the Areachap arc, along and adjacent to the Wilgenhoutsdrif Group (Van Niekerk and Beukes, 2019) and the development of rift-related basins. The rift basins were infilled with coarse, immature, locally derived clastic sediments derived from the rift shoulders (Moen, 1987). These volcanic rocks made use of faults along the Brakbosch-Trooilapspan fault system for their propagation and emplacement.

The subsequent volcanism occurred due to lithospheric thinning, which was likely caused by continued rifting and collapse after ocean closure (Fig. 14). The thinning caused partial melting of the subduction-influenced mantle giving rise to medium- to high-K tholeiitic mafic magmas which then rose. Some crustal assimilation along with crystal fractionation of the mafic magmas during ascent occurred to give rise to rhyolitic porphyries of the lower volcanic succession at ~1.13 Ga (Bailie et al.,

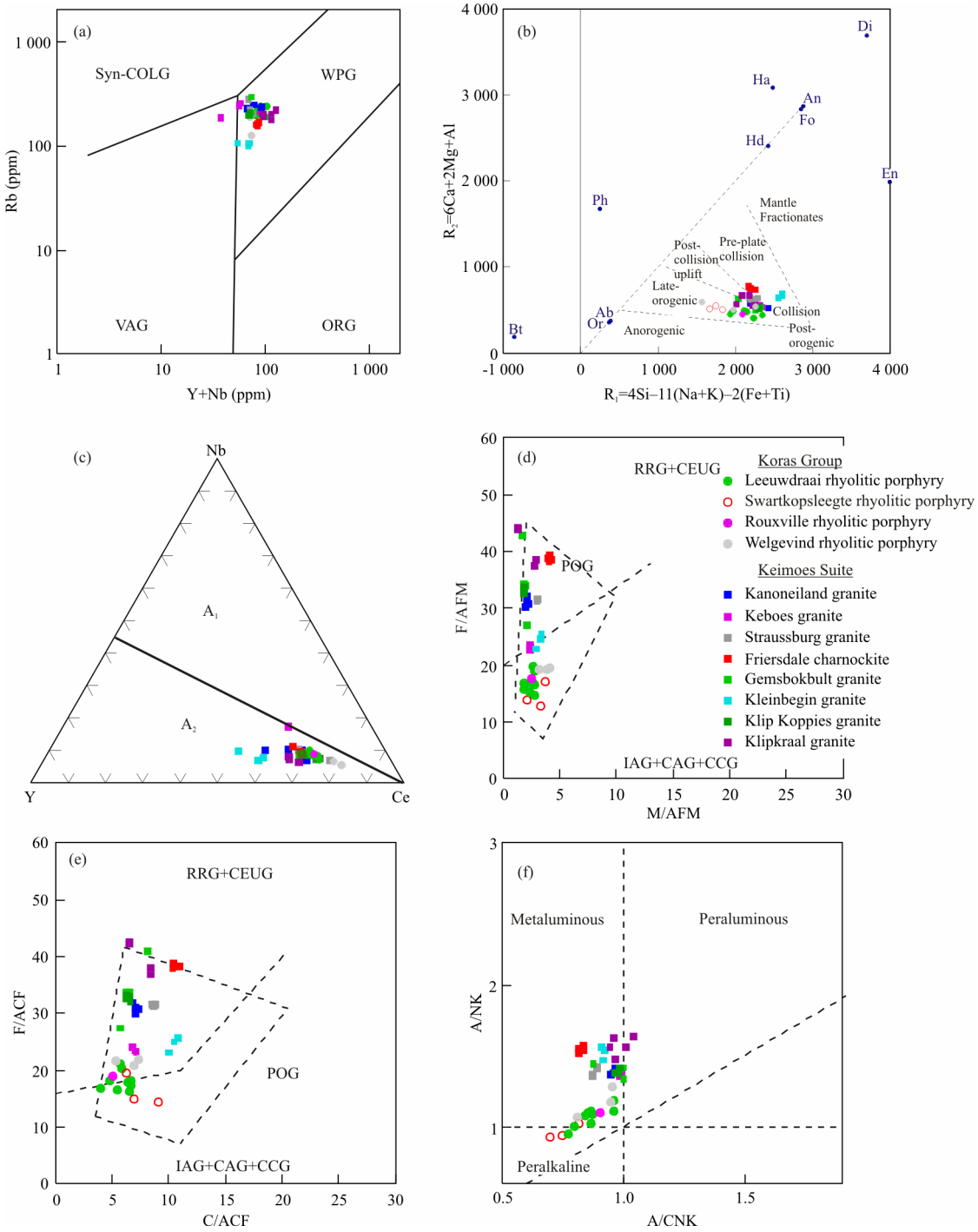

Figure 14. Geotectonic setting plots for the granites of the Keimoes Suite and rhyolitic porphyries of the Koras Group, eastern NMP. (a) The Y+Nb vs. Rb plot (after Pearce et al., 1984). (b) R_1-R_2 granite tectonic setting plot of Batchelor and Bowden (1985). (c) The Y-Nb-Ce ternary A-type granite classification plot of Eby (1992). (d)–(f) The granite tectonic discrimination plots of Maniar and Piccoli (1989). WPG. Within-plate granite; VAG. volcanic-arc granite; ORG. ocean ridge granite; syn-COLG. syn-collisional granite; IAG. island arc granitoids; CAG. continental arc granitoids; CCG. continental collision granitoids; POG. post-orogenic granitoids; RRG. rift-related granitoids; CEUG. continental epeirogenic uplift granitoids; OP. ocean plagiogranites; IAG, CAG, CCG, POG are orogenic granitoids; RRG, CEUG, OP are anorogenic granitoids.

2012) (seen in the high concentrations of the LIL and HFS elements) during the waning of the peak metamorphic conditions and prior to, and at the onset of the main D_2 deformation phase. This is evident from the similar trace element characteristics of both basaltic andesites and rhyolitic porphyries, and their $\varepsilon_{Nd}(t)$ values that vary from positive to weakly negative.

Subsequent melting occurred at ~1.1 Ga. This was likely unrelated to any plume activity (e.g., De Kock et al., 2014), but was likely due to continued and/or renewed rifting (slab break-off?). The voluminous magmatism was accompanied by lower grade M_3 metamorphism (at ~1.12–1.08 Ga). Mantle melting gave rise to the basaltic andesites of the upper succession of the Koras Group that intruded the lower to mid-crust bringing about copious melting and the generation of the various Keimoes

Suite granites. The emplacement of these mafic magmas at various crustal levels, as now exposed at the Oranjekom Complex in the Kakamas Domain, led to local heating and crustal melting giving rise to the generation of crust-derived felsic magmas, represented by the rhyolitic porphyries of the upper succession of the Koras Group, as denoted by their negative $\varepsilon_{Nd}(t)$ values and strongly enriched trace element concentrations relative to PM. Crustal magma chambers experienced renewed magma input, as evidenced in the resorbed phenocrysts in the rhyolitic porphyries (Figs. 3b, 3d). The Keimoes Suite ended with the Friersdale charnockite, the youngest and most voluminous member, centred along the BoSZ suggesting that the latter formed the locus and conduit of the late- to post-tectonic intrusive magmatism. The post-tectonic Friersdale charnockite made use of pre-existing F_1 and F_2 hinge zones for its intrusion (Mathee, 2017).

The granites of the Keimoes Suite, emplaced at depths of >15 km, and the Areachap Group, which experienced upper amphibolite facies metamorphic conditions, are adjacent to the bimodal volcanics of the Koras Group and mafic volcanics of the Wilgenhoutsdrif Group, both of which were only subjected to greenschist facies metamorphism. Continued south-westward-directed movement of the Kaapvaal Craton into the NMP subsequent to ~1.11–1.08 Ga created flower structures associated with dextral strike-slip movement (Jacobs et al., 1993; van Bever Donker, 1991). This occurred between 1 024 and 1 018 Ma (D_4 deformation; Mathee, 2017). Substantial exhumation and vertical displacement (of ~12–20 km) must have occurred to create this juxtaposition, giving rise to a positive pop-up flower structure. This uplift was focussed along prominent thrusts, which were subsequently reactivated as shear zones. Examples of reactivated faults include the regionally significant Blauwboschpan and Brakbosch faults, and Trooilapspan and Neusspruit shear zones, the former two forming the present-day boundaries of the Koras Group to the east and west respectively. The Keimoes Suite was exposed due to uplift in a positive flower structure. By contrast, the Koras Group is preserved within a negative flower structure due to the development of graben-like structures.

The *P-T* paths do not suggest pressures above 6–8 kbar (equivalent of 22–30 km depth for a geotherm of ~25 °C/km) for the Areachap Group (e.g., Bachmann et al., 2015), suggesting thicknesses of no more than 50 km for the western margin of the Kaapvaal Craton. Closure of a narrow ocean, represented by the Areachap Sea, and accretion of this arc onto the thinned western margin of the Kaapvaal Craton would have caused thickening of no more than 50 km, rather than to more than 70 km. The latter would be the case in a Himalayan-style continental collision scenario, which is not envisioned here. Thrust stacking is, therefore, a more likely scenario compared to crustal thickening. The positive flower structure of the Kakamas and Areachap Domains (Fig. 2), with eastward-directed thrusting into the Kheis terrane (Van Niekerk and Beukes, 2019) and westward-directed thrusting along the Hartbees River Thrust of the Kakamas Domain over the BSP, also suggests closure of a narrow ocean.

6 CONCLUSIONS

The granites of the Keimoes Suite formed largely by melting of crustal material of mainly mafic igneous sources, with a minor sedimentary component, as seen in their isotopic and whole-rock major- and trace-element data. The spread of $\varepsilon_{Nd}(t)$ values and variable model ages suggest derivation from variable degrees of mixing between predominantly Paleoproterozoic crustal material and juvenile Mesoproterozoic sources. In some granites a suggestion of a mantle source component is present. Mafic mantle-derived melts also acted as a source of advective heat and as potential participants in hybrid magma generation. This is seen in the low positive $\varepsilon_{Nd}(t)$ values near zero for some granites, such as the Friersdale charnockite, but assimilation of variably aged crustal material explains the large range in initial Sr isotope values. Magmatism was due to transtensional rifting and asthenospheric upwelling.

Following closure of the Areachap Sea, late Namaquan transcurrent movements led to decompression melting in the mantle, giving rise to the intrusion of mafic bodies, preferentially into the lower to mid-crust. These intrusions transferred heat, leading to melting of this crust, likely of a multi-layered nature involving components of mostly Paleoproterozoic-aged crust of the NMP interspersed with Mesoproterozoic arc material and lesser Archean to Paleoproterozoic material of the Kaapvaal Craton. This melting then gave rise to the mixed hybrid magmas of the Keimoes Suite. The granitoids have mostly I-type characteristics, but also exhibit certain geochemical features more typical of A-type granites reflecting derivation from, and emplacement within a post-kinematic rift-related tectonic environment.

The lower succession of the Koras Group was derived by partial melting of subduction-influenced metasomatized, enriched mantle, with fractional crystallisation giving rise to the rhyolitic porphyries. By contrast, the upper succession rhyolites were derived by partial melting of Paleoproterozoic-aged crustal material. The bimodal volcanism was derived by rifting associated with and subsequent to Areachap Sea closure and arc accretion on the western margin of the Kaapvaal Craton due to continued southwest-directed movement of the latter into the NMP.

More detailed, in-depth studies of both the Keimoes Suite granitoids and rhyolitic porphyries of the Koras Group are necessary to clearly elucidate their sources and petrogenetic processes influencing their compositional variation. This review highlights the role of post-kinematic transtensional rifting in bringing about lithospheric thinning and partial melting giving rise to mafic magmas that can fractionate to give rise to felsic magmas. Intrusion of mafic magmas into the lower crust can also generate copious amounts of felsic crustal melts in such a post-kinematic environment.

ACKNOWLEDGMENTS

Thanks to Dr. Petrus le Roux of the Department of Geological Sciences, University of Cape Town for analysing the new set of Rb-Sr and Sm-Nd isotopes for the Koras Group volcanic rocks. Richard Harrison and Janine Botha of the Department of Earth Sciences, UWC are thanked for assistance with crushing and milling of samples for isotopic analysis. UWC International Conference Senate Research funds, which allowed RB to attend the IXth Hutton Symposium on Granites and Related Rocks in Nanjing, China in 2019, are gratefully acknowledged. Reviews by two anonymous reviewers, and a constructive review by special volume editor, Valdecir de Assis Janasi, are gratefully ac-

knowledged. The final publication is available at Springer via https://doi.org/10.1007/s12583-021-1462-7.

Electronic Supplementary Materials: Supplementary materials containing analytical techniques (ESM1), figures (ESM2), Table S1 (ESM3) are available in the online version of this article at https://doi.org/10.1007/s12583-021-1462-7.

REFERENCES CITED

Bachmann, K., Schulz, B., Bailie, R., et al., 2015. Monazite Geochronology and Geothermobarometry in Polymetamorphic Host Rocks of Volcanic-Hosted Massive Sulphide Mineralizations in the Mesoproterozoic Areachap Terrane, South Africa. *Journal of African Earth Sciences*, 111: 258–272. https://doi.org/10.1016/j.jafrearsci.2015.07.021

Bachmann, O., Miller, C. F., de Silva, S. L., 2007. The Volcanic-Plutonic Connection as a Stage for Understanding Crustal Magmatism. *Journal of Volcanology and Geothermal Research*, 167(1–4): 1–23. https://doi.org/10.1016/j.jvolgeores.2007.08.002

Bailie, R., Gutzmer, J., Rajesh, H. M., 2010. Lithogeochemistry as a Tracer of the Tectonic Setting, Lateral Integrity and Mineralization of a Highly Metamorphosed Mesoproterozoic Volcanic Arc Sequence on the Eastern Margin of the Namaqua Province, South Africa. *Lithos*, 119(3/4): 345–362. https://doi.org/10.1016/j.lithos.2010.07.012

Bailie, R., Gutzmer, J., Rajesh, H. M., et al., 2011a. Age of Ferroan A-Type Post-Tectonic Granitoids of the Southern Part of the Keimoes Suite, Northern Cape Province, South Africa. *Journal of African Earth Sciences*, 60(3): 153–174. https://doi.org/10.1016/j.jafrearsci.2011.02.008

Bailie, R., Gutzmer, J., Rajesh, H. M., 2011b. Petrography, Geochemistry and Geochronology of the Metavolcanic Rocks of the Mesoproterozoic Leerkrans Formation, Wilgenhoutsdrif Group, South Africa—Back-Arc Basin to the Areachap Volcanic Arc. *South African Journal of Geology*, 114(2): 167–194. https://doi.org/10.2113/gssajg.114.2.167

Bailie, R., Rajesh, H. M., Gutzmer, J., 2012. Bimodal Volcanism at the Western Margin of the Kaapvaal Craton in the Aftermath of Collisional Events during the Namaqua-Natal Orogeny: The Koras Group, South Africa. *Precambrian Research*, 200–203: 163–183. https://doi.org/10.1016/j.precamres.2012.01.017

Bailie, R., Macey, P. H., Nethenzheni, S., et al., 2017. The Keimoes Suite Redefined: The Geochronological and Geochemical Characteristics of the Ferroan Granites of the Eastern Namaqua Sector, Mesoproterozoic Namaqua-Natal Metamorphic Province, Southern Africa. *Journal of African Earth Sciences*, 134: 737–765. https://doi.org/10.1016/j.jafrearsci.2017.07.017

Barth, A. P., Feilen, A. D. G., Yager, S. L., et al., 2012. Petrogenetic Connections between Ash-Flow Tuffs and a Granodioritic to Granitic Intrusive Suite in the Sierra Nevada Arc, California. *Geosphere*, 8(2): 250–264. https://doi.org/10.1130/ges00737.1

Batchelor, R. A., Bowden, P., 1985. Petrogenetic Interpretation of Granitoid Rock Series Using Multicationic Parameters. *Chemical Geology*, 48(1–4): 43–55. https://doi.org/10.1016/0009-2541(85)90034-8

Becker, H., Jochum, K. P., Carlson, R. W., 2000. Trace Element Fractionation during Dehydration of Eclogites from High-Pressure Terranes and the Implications for Element Fluxes in Subduction Zones. *Chemical Geology*, 163(1–4): 65–99. https://doi.org/10.1016/s0009-2541(99)00071-6

Bial, J., Büttner, S. H., Frei, D., 2015. Formation and Emplacement of Two Contrasting Late-Mesoproterozoic Magma Types in the Central Namaqua Metamorphic Complex (South Africa, Namibia): Evidence from Geochemistry and Geochronology. *Lithos*, 224/225: 272–294. https://doi.org/10.1016/j.lithos.2015.02.021

Bogaerts, M., Scaillet, B., Auwera, J. V., 2006. Phase Equilibria of the Lyngdal Granodiorite (Norway): Implications for the Origin of Metaluminous Ferroan Granitoids. *Journal of Petrology*, 47(12): 2405–2431. https://doi.org/10.1093/petrology/egl049

Chiaradia, M., 2015. Crustal Thickness Control on Sr/Y Signatures of Recent Arc Magmas: An Earth Scale Perspective. *Scientific Reports*, 5: 8115. https://doi.org/10.1038/srep08115

Clemens, J. D., Stevens, G., 2012. What Controls Chemical Variation in Granitic Magmas? *Lithos*, 134/135: 317–329. https://doi.org/10.1016/j.lithos.2012.01.001

Clemens, J. D., Stevens, G., Farina, F., 2011. The Enigmatic Sources of I-Type Granites: The Peritectic Connexion. *Lithos*, 126(3/4): 174–181. https://doi.org/10.1016/j.lithos.2011.07.004

Cornell, D. H., Pettersson, A., 2007. Ion Probe Zircon Dating of Metasediments from the Areachap and Kakamas Terranes, Namaqua-Natal Province and the Stratigraphic Integrity of the Areachap Group. *South African Journal of Geology*, 110(4): 575–584. https://doi.org/10.2113/gssajg.110.4.575

Cornell, D. H., Kröner, A., Humphreys, H. C., et al., 1990. Age of Origin of the Polymetamorphosed Copperton Formation, Namaqua-Natal Province, Determined by Single Grain Zircon Pb-Pb Dating. *South African Journal of Geology*, 93(5): 709–716

Cornell, D. H., Thomas, R. J., Moen, H. F. G., et al., 2006. The Namaqua-Natal Province. In: Johnson, M. R., Anhaeusser, C. R., Thomas, R. J., eds., The Geology of South Africa. Council for Geoscience, Geological Society of South Africa. 325–379

Cornell, D. H., Pettersson, Å., Simonsen, S. L., 2012. Zircon U-Pb Emplacement and Nd-Hf Crustal Residence Ages of the Straussburg Granite and Friersdale Charnockite in the Namaqua-Natal Province, South Africa. *South African Journal of Geology*, 115(4): 465–484. https://doi.org/10.2113/gssajg.115.4.465

Cox, K. G., Bell, J. D., Pankhurst, R. J., 1979. The Interpretation of Igneous Rocks. George, Allen and Unwin, London. 450

De Kock, M. O., Ernst, R., Söderlund, U., et al., 2014. Dykes of the 1.11 Ga Umkondo LIP, Southern Africa: Clues to a Complex Plumbing System. *Precambrian Research*, 249: 129–143. https://doi.org/10.1016/j.precamres.2014.05.006

Eby, G. N., 1992. Chemical Subdivision of the A-Type Granitoids: Petrogenetic and Tectonic Implication. *Geology*, 20: 641–644. https://doi.org/10.1130/0091-7613(1992)020<0641:csotat>2.3.co;2

Eglington, B. M., 2006. Evolution of the Namaqua-Natal Belt, Southern Africa—A Geochronological and Isotope Geochemical Review. *Journal of African Earth Sciences*, 46(1/2): 93–111. https://doi.org/10.1016/j.jafrearsci.2006.01.014

Evans, D. A. D., Gutzmer, J., Beukes, N. J., et al., 2001. Paleomagnetic Constraints on Ages of Mineralization in the Kalahari Manganese Field, South Africa. *Economic Geology*, 96(3): 621–631. https://doi.org/10.2113/gsecongeo.96.3.621

Frost, C. D., Frost, B. R., 2011. On Ferroan (A-Type) Granitoids: Their Compositional Variability and Modes of Origin. *Journal of Petrology*, 52(1): 39–53. https://doi.org/10.1093/petrology/egq070

Frost, B. R., Barnes, C. G., Collins, W. J., et al., 2001. A Geochemical Classification for Granitic Rocks. *Journal of Petrology*, 42(11): 2033–2048. https://doi.org/10.1093/petrology/42.11.2033

Gagnevin, D., Daly, J. S., Kronz, A., 2010. Zircon Texture and Chemical Composition as a Guide to Magmatic Processes and Mixing in a Granitic Environment and Coeval Volcanic System. *Contributions to Mineralogy and Petrology*, 159(4): 579–596. https://doi.org/10.1007/s00410-009-0443-0

Geringer, G. J., Botha, B. J. V., Pretorius, J. J., et al., 1986. Calc-Alkaline Volcanism along the Eastern Margin of the Namaqua Mobile Belt, South Africa—A Pos-

sible Middle Proterozoic Volcanic Arc. *Precambrian Research*, 33(1–3): 139–170. https://doi.org/10.1016/0301-9268(86)90019-7

Geringer, G. J., De Bruiyn, H., Schoch, A. E., et al., 1987. The Geochemistry and Petrogenetic Relationships of Two Granites and Their Inclusions in the Keimoes Suite of the Namaqua Mobile Belt, South Africa. *Precambrian Research*, 36(2): 143–162. https://doi.org/10.1016/0301-9268(87)90086-6

Geringer, G. J., Botha, B. J. V., Slabbert, M. J., 1988. The Keimoes Suite—A Composite Granitoid Batholith along the Eastern Margin of the Namaqua Mobile Belt, South Africa. *South African Journal of Geology*, 91(4): 465–476

Geringer, G. J., Humphreys, H. C., Scheepers, D. J., 1994. Lithostratigraphy, Protolithology, and Tectonic Setting of the Areachap Group along the Eastern Margin of the Namaqua Mobile Belt, South Africa. *South African Journal of Geology*, 97(1): 78–100

Gutzmer, J, J., Beukes, N. J., Pickard, A., et al., 2000. 1 170 Ma SHRIMP Age for Koras Group Bimodal Volcanism, Northern Cape Province. *South African Journal of Geology*, 103(1): 32–37. https://doi.org/10.2113/103.1.32

Humphreys, H. C., van Bever Donker, J. M., 1990. Early Namaqua Low-Pressure Metamorphism: Deformation and Porphyroblast Growth in the Zoovoorby Staurolite Schist, South Africa. *Journal of Metamorphic Geology*, 8(2): 159–170. https://doi.org/10.1111/j.1525-1314.1990.tb00463.x

Jacobs, J., Thomas, R. J., Weber, K., 1993. Accretion and Indentation Tectonics at the Southern Edge of the Kaapvaal Craton during the Kibaran (Grenville) Orogeny. *Geology*, 21(3): 203–206. https://doi.org/10.1130/0091-7613(1993)0210203:aaitat>2.3.co;2

Jacobs, J., Pisarevsky, S., Thomas, R. J., et al., 2008. The Kalahari Craton during the Assembly and Dispersal of Rodinia. *Precambrian Research*, 160(1/2): 142–158. https://doi.org/10.1016/j.precamres.2007.04.022

Jung, S., Mezger, K., Nebel, O., et al., 2012. Origin of Meso-Proterozoic Post-Collisional Leucogranite Suites (Kaokoveld, Namibia): Constraints from Geochronology and Nd, Sr, Hf, and Pb Isotopes. *Contributions to Mineralogy and Petrology*, 163(1): 1–17. https://doi.org/10.1007/s00410-011-0655-y

Kruger, F. J., Geringer, G. J., Havenga, A. T., 2000. The Geology, Petrology, Geochronology and Source Region Character of the Layered Gabbronoritic Oranjekom Complex in the Kibaran Namaqua Mobile Belt, South Africa. *Journal of African Earth Sciences*, 30(3): 675–687. https://doi.org/10.1016/s0899-5362(00)00045-2

La Flèche, M. R., Camiré, G., Jenner, G. A., 1998. Geochemistry of Post-Acadian, Carboniferous Continental Intraplate Basalts from the Maritimes Basin, Magdalen Islands, Québec, Canada. *Chemical Geology*, 148(3/4): 115–136. https://doi.org/10.1016/s0009-2541(98)00002-3

Laurent, O., Martin, H., Moyen, J. F., et al., 2014. The Diversity and Evolution of Late-Archean Granitoids: Evidence for the Onset of "Modern-Style" Plate Tectonics between 3.0 and 2.5 Ga. *Lithos*, 205: 208–235. https://doi.org/10.1016/j.lithos.2014.06.012

Le Maitre, R. W., Bateman, P., Dudek, A., et al., 1989. A Classification of Igneous Rocks and Glossary of Terms. Blackwell, Oxford

Li, Z. X., Bogdanova, S. V., Collins, A. S., et al., 2008. Assembly, Configuration, and Break-up History of Rodinia: A Synthesis. *Precambrian Research*, 160(1/2): 179–210. https://doi.org/10.1016/j.precamres.2007.04.021

Macey, P. H., Siegfried, H. P., Minnaar, H., et al., 2011. The Geology of the Loeriesfontein Area—1 : 250 000 Map Sheet Explanation, Sheet 3018. Council for Geoscience, Pretoria. 152

Macey, P. H., Thomas, R. J., Minnaar, H. M., et al., 2017. Origin and Evolution of the ~1.9 Ga Richtersveld Magmatic Arc, SW Africa. *Precambrian Research*, 292: 417–451. https://doi.org/10.1016/j.precamres.2017.01.013

Macey, P. H., Bailie, R. H., Miller, J. A., et al., 2018. Implications of the Distribution, Age and Origins of the Granites of the Mesoproterozoic Spektakel Suite for the Timing of the Namaqua Orogeny in the Bushmanland Subprovince of the Namaqua-Natal Metamorphic Province, South Africa. *Precambrian Research*, 312: 68–98. https://doi.org/10.1016/j.precamres.2018.02.026

Maniar, P. D., Piccoli, P. M., 1989. Tectonic Discrimination of Granitoids. *Geological Society of America Bulletin*, 101(5): 635–643. https://doi.org/10.1130/0016-7606(1989)1010635: tdog>2.3.co;2

Mathee, H. L. M., 2017. Structural-Stratigraphic Investigation of an Area near Kakamas and Environs, Namaqua Mobile Belt, South Africa: [Dissertation]. University of the Free State, Bloemfontein. 192

McCulloch, M. T., Gamble, J. A., 1991. Geochemical and Geodynamical Constraints on Subduction Zone Magmatism. *Earth and Planetary Science Letters*, 102(3/4): 358–374. https://doi.org/10.1016/0012-821x(91)90029-h

McDonough, W. F., Sun, S. S., 1995. The Composition of the Earth. *Chemical Geology*, 120(3/4): 223–253. https://doi.org/10.1016/0009-2541(94)00140-4

Moen, H. F. G., 1987. The Koras Group and Related Intrusives North of Upington: A Reinvestigation. *Bulletin of the Geological Survey of South Africa*, 85: 20

Moen, H. F. G., 1999. The Kheis Tectonic Subprovince, Southern Africa: A Lithostratigraphic Perspective. *South African Journal of Geology*, 102(1): 27–42

Moen, H. F. G., 2007. The Geology of the Upington Area. Explanation, Map Sheet 2820 (Scale 1 : 250 000). South African Council for Geoscience, Pretoria. 160

Moen, H. F. G., Toogood, D. J., 2007. The Geology of the Onseepkans Area. Map and Explanation, Sheet 2818 Onseepkans (1 : 250 000). South African Council for Geoscience, Pretoria. 101

Mothibi, K. N., 2016. A Re-assessment of the Age of the Lower Koras Group: [Dissertation]. University of the Western Cape, Bellville. 32

Nke, A. Y., Bailie, R. H., Macey, P. H., et al., 2020. The 1.8 Ga Gladkop Suite: The Youngest Palaeoproterozoic Domain in the Namaqua-Natal Metamorphic Province, South Africa. *Precambrian Research*, 350: 105941. https://doi.org/10.1016/j.precamres.2020.105941

O'Connor, J. T., 1965. A Classification of Quartz-Rich Igneous Rocks Based on Feldspar Ratio. *Geological Survey Professional Paper*, 525: B79–B84

Patiño Douce, A. E., 1997. Generation of Metaluminous A-Type Granites by Low-Pressure Melting of Calc-Alkaline Granitoids. *Geology*, 25(8): 743–746. https://doi.org/10.1130/0091-7613(1997)0250743:gomatg>2.3.co;2

Patiño Douce, A. E., 1999. What do Experiments Tell us about the Relative Contributions of Crust and Mantle to the Origin of Granitic Magmas?. *Geological Society*, *London*, *Special Publications*, 168(1): 55–75. https://doi.org/10.1144/gsl.sp.1999.168.01.05

Patiño Douce, A. E., Harris, N., 1998. Experimental Constraints on Himalayan Anatexis. *Journal of Petrology*, 39(4): 689–710. https://doi.org/10.1093/petroj/39.4.689

Pearce, J. A., Harris, N. B. W., Tindle, A. G., 1984. Trace Element Discrimination Diagrams for the Tectonic Interpretation of Granitic Rocks. *Journal of Petrology*, 25(4): 956–983. https://doi.org/10.1093/petrology/25.4.956

Peccerillo, A., Barberio, M. R., Yirgu, G., et al., 2003. Relationships between Mafic and Peralkaline Silicic Magmatism in Continental Rift Settings: A Petrological, Geochemical and Isotopic Study of the Gedemsa Volcano, Central Ethiopian Rift. *Journal of Petrology*, 44(11): 2003–2032. https://doi.org/10.1093/petrology/egg068

Pettersson, Å., 2008. Mesoproterozoic Crustal Evolution in Southern Africa. [Dissertation]. Gothenburg University, Gothenburg. A117

Pettersson, Å., Cornell, D. H., Moen, H. F. G., et al., 2007. Ion-Probe Dating of 1.2 Ga Collision and Crustal Architecture in the Namaqua-Natal

Province of Southern Africa. *Precambrian Research*, 158(1/2): 79–92. https://doi.org/10.1016/j.precamres.2007.04.006

Pettersson, Å., Cornell, D. H., Yuhara, M., et al., 2009. Sm-Nd Data for Granitoids across the Namaqua Sector of the Namaqua-Natal Province, South Africa. *Geological Society*, *London*, *Special Publications*, 323(1): 219–230. https://doi.org/10.1144/sp323.10

Rollinson, H. R., 1993. Using Geochemical Data: Evaluation, Presentation, Interpretation. Longman Scientific and Technical, Harlow. 352

Sanderson-Damstra, C. G., 1982. Geology of the Central and Southern Domains of the Koras Group, Northern Cape Province: [Dissertation]. Rhodes University, Grahamstown

Seghedi, I., Besutiu, L., Mirea, V., et al., 2019. Tectono-Magmatic Characteristics of Post-Collisional Magmatism: Case Study East Carpathians, Călimani-Gurghiu-Harghita Volcanic Range. *Physics of the Earth and Planetary Interiors*, 293: 106270. https://doi.org/10.1016/j.pepi.2019.106270

Sithole, N., 2013. A Study into the Main Structural Features of the Namaqua Region and Their Relation to the Intrusion of the Keimoes Suite: [Dissertation]. University of the Western Cape, Bellville. 85

Skjerlie, K. P., Johnston, A. D., 1993. Fluid-Absent Melting Behavior of an F-Rich Tonalitic Gneiss at Mid-Crustal Pressures: Implications for the Generation of Anorogenic Granites. *Journal of Petrology*, 34(4): 785–815. https://doi.org/10.1093/petrology/34.4.785

Stevens, G., Villaros, A., Moyen, J.-F., 2007. Selective Peritectic Garnet Entrainment as the Origin of Geochemical Diversity in S-Type Granites. *Geology*, 35(1): 9–12. https://doi.org/10.1130/g22959a.1

Stowe, C. W., 1983. The Upington Geotraverse and Its Implications for Craton Margin Tectonics. In: Botha, B. J. V., ed., Namaqualand Metamorphic Complex. *Special Publication of the Geological Society of South Africa*, 10: 147–171

Sylvester, P. J., 1998. Post-Collisional Strongly Peraluminous Granites. *Lithos*, 45(1–4): 29–44. https://doi.org/10.1016/s0024-4937(98)00024-3

Sun, S. S., McDonough, W. F., 1989. Chemical and Isotopic Systematics of Oceanic Basalts: Implications for Mantle Composition and Processes. *Geological Society*, *London*, *Special Publications*, 42(1): 313–345. https://doi.org/10.1144/gsl.sp.1989.042.01.19

Thomas, R. J., Agenbacht, A. L. D., Cornell, D. H., et al., 1994. The Kibaran of Southern Africa: Tectonic Evolution and Metallogeny. *Ore Geology Reviews*, 9(2): 131–160. https://doi.org/10.1016/0169-1368(94)90025-6

Thomas, R. J., Macey, P. H., Spencer, C., et al., 2016. The Sperrgebiet Domain, Aurus Mountains, SW Namibia: A ~2 020–850 Ma Window within the Pan-African Gariep Orogen. *Precambrian Research*, 286: 35–58. https://doi.org/10.1016/j.precamres.2016.09.023

van Bever Donker, J. M., 1980. Structural and Metamorphic Evolution of an Area around Kakamas and Keimoes, Cape Province, South Africa. *Bulletin of the Precambrian Research Unit*, *University of Cape Town*, 28: 165

van Bever Donker, J. M., 1991. A Synthesis of the Structural Geology of a Major Tectonic Boundary between a 1 000 M.y. Mobile Belt and a 3 000 M.y. Craton. *Tectonophysics*, 196(3/4): 359–370. https://doi.org/10.1016/0040-1951(91)90330-u

Van Niekerk, H. S., 2006. The Origin of the Kheis Terrane and Its Relationship with the Archean Kaapvaal Craton under the Grenvillian Namaqua Province in Southern Africa: [Dissertation]. University of Johannesburg, Johannesburg. 402

Van Niekerk, H. S., Beukes, N. J., 2019. Revised Definition/Outline of the Kheis Terrane along the Western Margin of the Kaapvaal Craton and Lithostratigraphy of the Newly Proposed Keis Supergroup. *South African Journal of Geology*, 122(2): 187–220. https://doi.org/10.25131/sajg.122.0014

Villaros, A., Stevens, G., Moyen, J. F., et al., 2009. The Trace Element Compositions of S-Type Granites: Evidence for Disequilibrium Melting and Accessory Phase Entrainment in the Source. *Contributions to Mineralogy and Petrology*, 158(4): 543–561. https://doi.org/10.1007/s00410-009-0396-3

Villaseca, C., Barbero, L., Herreros, V., 1998. A Re-Examination of the Typology of Peraluminous Granite Types in Intracontinental Orogenic Belts. *Transactions of the Royal Society of Edinburgh*: *Earth Sciences*, 89(2): 113–119. https://doi.org/10.1017/s0263593300007045

Weaver, B. L., Tarney, J., 1984. Empirical Approach to Estimating the Composition of the Continental Crust. *Nature*, 310(5978): 575–577. https://doi.org/10.1038/310575a0

Whalen, J. B., Currie, K. L., Chappell, B. W., 1987. A-Type Granites: Geochemical Characteristics, Discrimination and Petrogenesis. *Contributions to Mineralogy and Petrology*, 95(4): 407–419. https://doi.org/10.1007/bf00402202

Yan, L. L., He, Z. Y., Beier, C., et al., 2018a. Geochemical Constraints on the Link between Volcanism and Plutonism at the Yunshan Caldera Complex, SE China. *Contributions to Mineralogy and Petrology*, 173: 4. https://doi.org/10.1007//s00410-017-1430-5

Yan, L. L., He, Z. Y., Beier, C., et al., 2018b. Zircon Trace Element Constrains on the Link between Volcanism and Plutonism in SE China. *Lithos*, 320/321: 28–34. https://doi.org/10.1016/j.lithos.2018.08.040